ARMY RESEARCH LABORATORY

Armor Plate Surface Roughness Measurements

by Brian Stanton, William Coburn,
and Thomas J. Pizzillo

ARL-TR-3498 April 2005

NOTICES

Disclaimers

The findings in this report are not to be construed as an official Department of the Army position unless so designated by other authorized documents.

Citation of manufacturer's or trade names does not constitute an official endorsement or approval of the use thereof.

Destroy this report when it is no longer needed. Do not return it to the originator.

Army Research Laboratory
Adelphi, MD 20783-1197

ARL-TR-3498 **April 2005**

Armor Plate Surface Roughness Measurements

Brian Stanton, William Coburn
and Thomas J. Pizzillo
Sensors and Electron Devices Directorate, ARL

REPORT DOCUMENTATION PAGE

Form Approved
OMB No. 0704-0188

1. REPORT DATE *(DD-MM-YYYY)*	2. REPORT TYPE	3. DATES COVERED (From - To)
April 2005	Final	March to October 2004

4. TITLE AND SUBTITLE
Armor Plate Surface Roughness Measurements

5a. CONTRACT NUMBER

5b. GRANT NUMBER

5c. PROGRAM ELEMENT NUMBER

6. AUTHOR(S)
Brian Stanton, William Coburn, and Thomas J. Pizzillo

5d. PROJECT NUMBER
5NE4I6

5e. TASK NUMBER

5f. WORK UNIT NUMBER

7. PERFORMING ORGANIZATION NAME(S) AND ADDRESS(ES)
U.S. Army Research Laboratory
ATTN: AMSRD-ARL-SE-RU
2800 Powder Mill Road
Adelphi, MD 20783-1197

8. PERFORMING ORGANIZATION REPORT NUMBER
ARL-TR-3498

9. SPONSORING/MONITORING AGENCY NAME(S) AND ADDRESS(ES)
U.S. Army Research Laboratory
2800 Powder Mill Road
Adelphi, MD 20783-1197

10. SPONSOR/MONITOR'S ACRONYM(S)

11. SPONSOR/MONITOR'S REPORT NUMBER(S)

12. DISTRIBUTION/AVAILABILITY STATEMENT
Approved for public release; distribution unlimited.

13. SUPPLEMENTARY NOTES

14. ABSTRACT
The accuracy and limitations of DoD high frequency radar signature prediction codes depend on the approximations included in the underlying algorithms. At K_a-Band and above, accurate representation of the target surfaces becomes a limiting factor in the electromagnetic simulation, since the resolution requirements are on the same order as fabrication tolerances. Even if accurate representations of test vehicles can be obtained, there may still be discrepancies in the modeled surface condition (i.e., surface texture and coatings) that could become important at high frequency. We measure waviness and roughness of various plates to know the parameter range for smooth aluminum and rolled homogenous armor (RHA). We also modify the plates by grit blasting to determine how parameters might change during surface preparation for painting. Using these roughness parameters and typical electrical characteristics for paint, we can estimate the effect of surface condition on RCS predictions at K_a-Band. For the painting process and surface roughness typical of ground vehicles, theory predicts only a small difference compared to smooth metal targets.

15. SUBJECT TERMS
Surface texture, roughness, RCS, RHA armor plates

16. SECURITY CLASSIFICATION OF:			17. LIMITATION OF ABSTRACT	18. NUMBER OF PAGES	19a. NAME OF RESPONSIBLE PERSON
a. REPORT	b. ABSTRACT	c. THIS PAGE			Brian Stanton
Unclassified	Unclassified	Unclassified	U	50	19b. TELEPHONE NUMBER (*Include area code*) (301) 394-0855

Standard Form 298 (Rev. 8/98)
Prescribed by ANSI Std. Z39.18

Contents

List of Figures v

List of Tables vi

Acknowledgements vii

Summary ix

1. Introduction 1

2 Purpose 2

3. Plates 2

3.1 Aluminum Plates 2

3.2 Rolled Homogenous Armor Plates....2

3.3 Plate Modifications....3

3.4 Surface Characterization Using Gage 2000R Coordinate Measuring Machine....4

3.5 Plate Measurement Results 5

3.5.1 Aluminum Plate Measurement Characteristics 6

3.5.2 RHA Plate Measurement Characteristics 8

3.5.3 RHA Plate 2-1 Measurement Characteristics after Grit Blasting....11

3.5.4 RHA Plate 2-3 Measurement Characteristics after Grit Blasting....13

3.5.5 RHA and Aluminum Plate Measurement Characteristics Summary 15

3.5.6 Approximating Surface Condition Standard Deviation for Modeling 16

4. Rough Surface Numerical Modeling 16

4.1 General 16

4.2. Modeling a Square Plate using Xpatch 17

4.3 Xpatch RCS Calculations for the Modeled Square Plate....18

5. Theoretical Calculations **19**

5.1 General 19

5.1.1 Modified PO Model RCS Calculations for a Square Plate 19

5.1.2 Effect of Roughness on Monostatic RCS Pattern 21

5.2 Thin Coatings Analysis 28

6. Conclusions **31**

7. Recommendations **31**

8. References **33**

Distribution List **35**

List of Figures

Figure 1. Four large RHA and aluminum plates with unmodified surfaces. 3
Figure 2. Small RHA and Aluminum Plates with Modified Surfaces. 4
Figure 3. Gage 2000R CMM. 5
Figure 4. Measured surface roughness of the large Al plate (smooth and highly polished)....6
Figure 5. Measured surface roughness of plate Al-1 (smooth and highly polished). 7
Figure 6. Measured surface roughness of plate Al-1 (after grit blasting). 7
Figure 7. Measured surface height distribution of plate Al-1 before and after (a) course and (b) fine grit blasting. 8
Figure 8. Measured surface roughness of RHA plate 2. 9
Figure 9. Measured surface roughness of RHA plate 2-1. 9
Figure 10. Measured surface height distribution of RHA plate 2-1, side A compared to Gaussian and exponential distributions. 10
Figure 11. Measured surface height distribution of RHA 2-1, side B compared to Gaussian and exponential distributions. 10
Figure 12. Measured surface roughness of RHA plate 2-1 after grit blasting. 11
Figure 13. Measured surface height distribution of RHA plate 2-1 before and after (a) course and (b) fine grit blasting. 12
Figure 14. Measured surface height distribution of RHA plate 2-1, side A after course grit blasting compared to Gaussian and exponential distributions. 12
Figure 15. Measured surface height distribution of RHA plate 2-1, side B after fine grit blasting compared to Gaussian and exponential distributions. 13
Figure 16. Measured surface roughness of RHA plate 2-3 after grit blasting. 14
Figure 17. Measured surface height distribution of RHA plate 2-3, side A after course grit blasting compared to Gaussian and exponential distributions. 14
Figure 18. Measured surface height distribution of RHA plate 2-3, side B after fine grit blasting compared to Gaussian and exponential distributions. 15
Figure 19. Xpatch facet models of a 3-inch square plate with faceted random rough surface having (a) h = 5 mils, l_c = 0.2 inch, (b) h = 5 mils, l_c = 2 inch, and (c) h = 50 mils, l_c = 0.2 inch. 17
Figure 20. Xpatch results for Gaussian roughness similar to RHA plate 2-1, side A at 34 GHz with faceted rough surface as a function of roughness height. 18
Figure 21. Xpatch results for Gaussian roughness similar to RHA plate 2-1, side A, at 34 GHz compared to Modified PO Model. 20
Figure 22. The effect of surface roughness with $h = s$ = 5 mils on the broadside return of a perfectly conducting square plate. 21

Figure 23. Effect of surface roughness on RCS for the statistics of RHA plate 2-1, side A at 34 GHz. 23
Figure 24. Effect of surface roughness on RCS for the statistics of RHA plate 2-1, side B at 34 GHz. 24
Figure 25. Effect of surface roughness on RCS for the statistics of RHA plate 2-3, side A after coarse grit blasting at 34 GHz. 25
Figure 26. Effect of surface roughness on RCS for the statistics of RHA plate 2-3, side B after fine grit blasting at 34 GHz. 25
Figure 27. Measured RCS patterns. 27
Figure 28. The effect of CARC on the specular reflection of a flat plate at 34 GHz versus incidence angle. 29
Figure 29. Effect of lossy dielectric coating on broadside reflectivity of flat plate versus frequency. 30
Figure 30. Xpatch results for Gaussian roughness similar to RHA plate 2-1, side A at 34 GHz with faceted rough surface and a single CARC layer. 30

List of Tables

Table 1. RHA and aluminum plates used during experiment. 3
Table 2. Gage 2000R performance specifications. 4
Table 3. Summary of plate statistics. 16

Acknowledgements

The authors would like to thank Mr. Dave Heiner (AMSRD-ARL-WM-MC) from the Army Research Laboratory (ARL) Experimental Fabrication/Welding Metal Shop located on Spesutie Island, Aberdeen Proving Ground (APG) for providing and cutting the RHA plates to the desired dimensions.

The authors would like to thank Mr. Timothy White from the ARL Machine Shop, Adelphi, MD for providing and cutting the aluminum plates used as a baseline reference.

The authors would also like to thank personnel from the ARL Weapons and Materials Research Directorate (WMRD) for coating the aluminum and RHA plates with CARC primer and paint.

INTENTIONALLY LEFT BLANK.

Summary

High frequency radar cross section (RCS) signatures can be strongly influenced by the surface texture of the material, i.e., surface roughness, waviness, and lay. Accurate models for the entire surface condition, including surface texture, material treatments, and outer coatings such as paint, may be required. In particular, simulating the surface condition of a ground based target in an operational environment may be an important aspect of high frequency RCS signature prediction. With this knowledge, researchers and developers will have a high degree of confidence in the model results without requiring as much validation through measurements and field tests, saving the U.S. Army time and cost. These savings will result in the fielding of new and/or improved weapon systems in a much shorter period. In an effort to explore the effect of surface texture on RCS predictions, we measured the waviness and roughness of plate targets. The primary objectives of this experiment were to a) characterize the surface texture of aluminum and RHA plates; b) determine how the surface texture is modified by standard grit blasting methods; and c) estimate the influence of surface condition, primarily random roughness and chemical agent resistant coating (CARC) on RCS predictions.

Aluminum plates were used as a smooth surface for a baseline reference, while rolled homogeneous armor (RHA) was considered the primary material. The aluminum plates were smooth and highly polished, while the RHA plates were heavily scaled and rusted. The roughness of the aluminum and RHA plates were measured using a Gage 2000R coordinate measuring machine (CMM). The roughness was statistically described, based on the CMM measurements, by determining the rms height, peak-to-valley height, $p = z_{pp}$, correlation length, l_c, and standard deviation, s, for each of the plates. The plates were then modified by grit blasting each plate with 100-170 μm size (course grit) glass beads on side A and 40-60 μm size (fine grit) glass beads on side B. The roughness of each plate was measured once again with the Gage 2000R and statistics were developed describing the roughness. We showed $s > 4$ mils for rusty RHA plates and that grit blasting reduces the standard deviation to $s \sim 2 - 3$ mils. There was a measurable difference with roughness due to grit sizes, but it was small. Either size was considered to represent the surface preparation for painting. In other words, although grit blasting altered the surface appearance, i.e., the surface height distribution was smoother after fine or course grit blasting, the changes did not produce a large effect on the surface roughness. All of the RHA and aluminum plates had approximately Gaussian statistics. This remained true even after grit blasting. A single aluminum plate and two RHA plates were then painted with CARC primer (MIL-P-53030) on side A and CARC green paint (MIL-DTL-64159) on Side B.

For numerical simulation, we used Xpatch to model a random rough surface. The Xpatch results were compared to a modified physical optics (PO) model. The effect of roughness on a monostatic RCS pattern was discussed. We also compared normal and exponential surface

distributions at K_a-Band. Measured RCS patterns using the K_a-Band monopulse radar are presented for both the aluminum and RHA plates.

Finally, we estimated the influence of surface condition, primarily a plate with random roughness and a coating of CARC on RCS predictions.

1. Introduction

The rapid acquisition cycle prescribed by the Army Transformation to future combat systems (FCS) makes radar signature simulations attractive for the design of next-generation military vehicles. High frequency radar cross section (RCS) signatures can be strongly influenced by the surface texture of the material i.e., surface roughness, waviness, and lay. Accurate models for the entire surface condition, including surface texture, material treatments, and outer coatings such as paint, may be required. For the Army to use radar signature predictions with confidence, the accuracy and limitations of high frequency algorithms must be well understood when applied to ground vehicles. In particular, simulating the surface condition of a ground based target in an operational environment may be an important aspect of high frequency RCS signature prediction. With this knowledge, researchers and developers will have a high degree of confidence in the model results without requiring as much validation through measurements and field tests, saving the U.S. Army time and cost. These savings will result in the fielding of new and/or improved weapon systems in a much shorter period.

In an effort to explore the effect of surface texture on RCS predictions, the waviness and roughness of plate targets were measured. Square plate facet models were created based on the measured surface roughness statistics. Xpatch[1], a DoD radar signature prediction analysis code suite based on physical optics (PO) and the shooting and bouncing ray (SBR) method (*1*), was used to generate RCS predictions for these plates. Predictions were done for a) smooth plates; b) smooth plates coated with chemical agent resistant coating (CARC); c) plates with rough surface; and d) plates with roughness and coated with CARC. The Xpatch predictions were compared to theoretical results at K_a-Band to determine the impact of surface roughness and CARC coatings on RCS.

This investigation used Aluminum (Al) plates and weathered rolled homogeneous armor (RHA) plates having rust and scale. There was a single 3 inch by 3 inch (small) aluminum plate, one 6 inch by 6 inch (large) aluminum plate, two 3 inch by 3 inch (small) RHA plates, and one 6 inch by 6 inch (large) RHA plate. Gage 2000R coordinate measuring machine (CMM) measurements showed each plate had slightly different surface texture with different surface roughness statistics. We present analytical and numerical results for backscatter by random rough surfaces and thin coatings such as CARC primer and paint. We describe our ability to modify and characterize the surface roughness and summarize Xpatch predictions compared to theoretical results. We include a plot of preliminary RCS data since a complete series of measurements under controlled conditions could not be arranged at this time.

[1] Xpatch® is a registered trademark of SAIC.

2 Purpose

The primary objectives were to a) characterize the surface texture of aluminum and RHA plates; b) determine how the surface texture is modified by standard grit blasting methods; and c) estimate the influence of surface condition, primarily random roughness and CARC on RCS predictions.

3. Plates

3.1 Aluminum Plates

The aluminum plates were used as a smooth surface for a baseline reference. A single 6 inch by 6 inch (large) aluminum plate; designated as plate Al, was cut into four 3 inch x 3 inch (small) aluminum plates with tolerances of ±3/1000 of an inch. One of the small aluminum plates, designated as plate Al-1, was used in this experiment. The aluminum plates were ½ inch thick.

3.2 Rolled Homogenous Armor Plates

Four 6 inch by 6 inch (large) RHA plates were cut from a single plate. A single large RHA plate, designated as plate RHA-2 was used in this experiment. This plate, RHA-2, was cut into four 3 inch by 3 inch (small) RHA plates with a tolerance of ±8/1000 of an inch. Two of the small RHA plates, designated as RHA 2-1 and RHA 2-3 were used in this experiment. The RHA plates were ¼ inch thick.

Figure 1 shows the four large RHA plates and the one large aluminum plate. RHA plate 1A, 2A, 3A, and 4A refer to the four RHA plates, side A. Aluminum plate A refers to side A of the aluminum plate. Ambient refers to the condition of the plates as obtained. For the RHA plates, the ambient condition was heavy scale and rust, while the ambient condition of the aluminum plate was smooth and highly polished. The waviness and roughness varied slightly between the RHA plates.

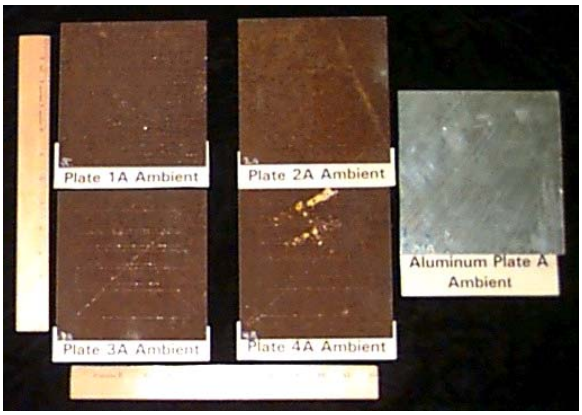

Figure 1. Four large RHA and aluminum plates with unmodified surfaces.

3.3 Plate Modifications

The aluminum plates were very smooth and highly polished on both sides. Aluminum plate Al-1 was modified by grit blasting the surface using 100-170 μm size (course grit) glass beads[2] on side A and then adding a layer of CARC paint[3]. Side B was modified by grit blasting the surface using 40-60 μm size (fine grit) glass beads and then adding a layer of CARC primer.

RHA plates 2-1 and 2-3 were modified by grit blasting the surface using course grit glass beads on side A and then adding a layer of CARC paint. Side B was modified by grit blasting the surface using fine grit glass beads and then adding a layer of CARC primer. Table 1 summarizes the plates used during the experiment.

Table 1. RHA and aluminum plates used during experiment.

Plate	Size (inches)	Status
Al	6x6	Smooth and highly polished
Al-1	3x3	Grit blasted CARC
RHA-2	6x6	Heavy scale and rust
2-1	3x3	Grit blasted CARC
2-3	3x3	Grit blasted CARC

[2] Cyclone Manufacturing, Dowagiac, MI (http://blasters.com/).

[3] by Army Research Laboratory (AMSRD-ARL-WM-MC) Aberdeen Proving Ground, MD.

Figure 2 shows several of the small RHA plates and the aluminum plate used as a smooth surface for a baseline reference. The plate on the top left is an RHA plate with heavy scale and rust. The plate on the top right is the very smooth and polished aluminum plate. The plate on the bottom left is an RHA plate with CARC primer (MIL-P-53030) and the bottom right is an RHA plate with CARC green paint (MIL-DTL-64159).

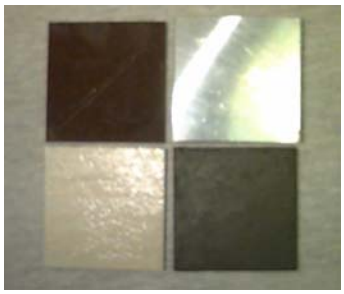

Figure 2. Small RHA and Aluminum Plates with Modified Surfaces.

3.4 Surface Characterization Using Gage 2000R Coordinate Measuring Machine

Usually the surface roughness of relatively smooth targets can be measured using standard stylus based measurement devices such as the Pocket Surf[4]. However, the RHA plates were too rough for this device, so the surface was measured using the Brown & Sharpe[5] Gage 2000R CMM. The Gage 2000R CMM integrates mechanical, pneumatic, and electronic features to achieve dimensional control, resulting in highly accurate coordinate measurements. The Gage 2000R CMM was used to measure X, Y, and Z coordinates of the RHA and aluminum plates to characterize the waviness and roughness. Gage 2000R performance specifications, reproduced from the Gage 2000R CCM Operator's Manual, are contained in table 2.

Table 2. Gage 2000R performance specifications.

Performance	Metric (mm)	English (Inches)
Repeatability	0.004	0.00016
Linear Accuracy	0.005	0.0002
Resolution	0.0000625	0.0000025

The Gage 2000R CMM features a granite tabletop spanned by an aluminum casting open web bridge. The Y-axis runs along the tabletop front to back, while the X-axis runs along the

[4] Mahr Federal, Inc., Providence, RI (http://www.mahrfederal.com/).

[5] Brown and Sharpe, Inc., North Kingstown, RI (http://www.brownandsharpe.com/).

tabletop left to right. The Z-axis is in the vertical direction. Air bearings are contained in each axis rail, providing near frictionless movement and support. Coordinates are measured with a spherical probe tip that contacts the surface of the plate. The probe is housed in a holder located at the bottom of the Z-rail. The Gage 2000R CMM interface is provided via a control box and VGA monitor. A serial port is located on the back of the control box, which was hooked up to a laptop computer for data recording. HyperTerminal[6] software was used to capture the coordinate data and then this file was imported to MatLab[7] for plotting and analysis. Figure 3 contains a photo of the Gage 2000R CMM.

Figure 3. Gage 2000R CMM.

3.5 Plate Measurement Results

The length, width, and thickness of the heavily scaled and rusted RHA plates and the aluminum plates were measured using calipers.

We measured the aluminum and RHA plates along a single path traversed across the plate diagonal using the Gage 2000R CMM. The surface height, z, was measured along the plate diagonal a minimum of three times to confirm that different measurements (i.e., slightly different paths) have similar statistics. The results presented are for a single measurement corresponding to a single realization of a random rough surface.

Measurements confirmed that the surface height varies randomly over each aluminum and RHA plate. Based on the CMM measurements, the plates have approximately zero mean height, although there can be some small variation in the plate thickness. A zero mean height was enforced for all plates by subtracting the average height from the data and then calculating the

[6] Hilgraeve Inc., Monroe, MI 48161 (http://www.hilgraeve.com).

[7] MathWorks, Natick, MA 01760 (http://www.mathworks.com).

rms surface height, $h = z_{rms}$. For small plates the waviness can be neglected. The surface roughness is approximated on a flat plate by superimposing zero mean height, two-dimensional, random roughness, so that the standard deviation is $s = h$. The rms height, peak-to-valley height, $p = z_{pp}$, and correlation length, l_c, are included as an inset in the graphs presented.

3.5.1 Aluminum Plate Measurement Characteristics

The Gage 2000 R CMM large aluminum plate measured surface roughness is shown in figure 4. The measured surface height indicates 3-4 mil variation in thickness over the plate diagonal with the two sides having opposite trends, as might be expected.

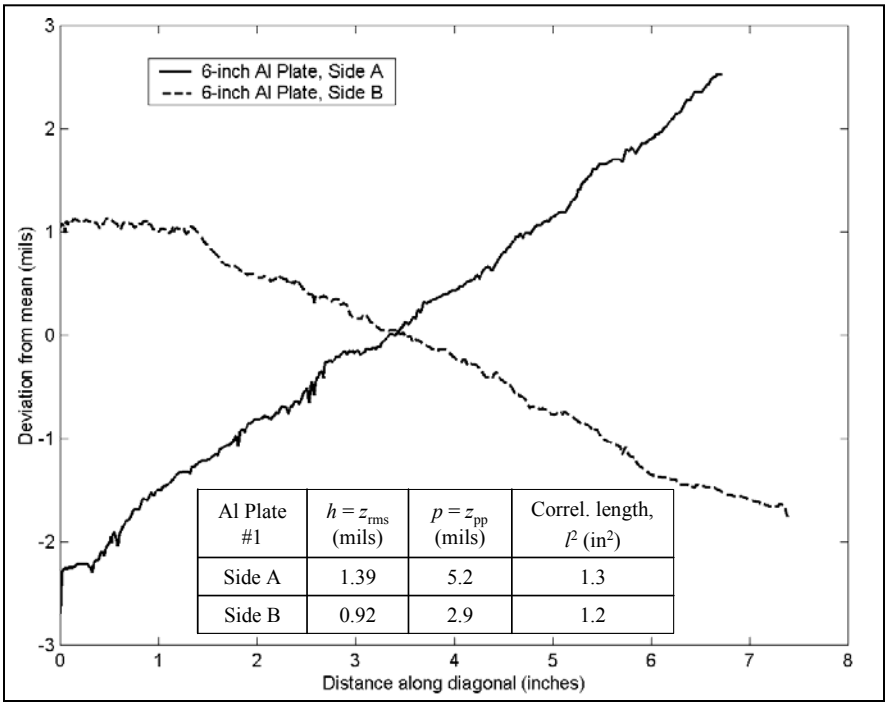

Al Plate #1	$h = z_{rms}$ (mils)	$p = z_{pp}$ (mils)	Correl. length, l^2 (in^2)
Side A	1.39	5.2	1.3
Side B	0.92	2.9	1.2

Figure 4. Measured surface roughness of the large Al plate (smooth and highly polished).

For the small aluminum plate, we see more of the same random variation as shown in figure 5, with smooth aluminum having s~0.2 mils. The same plate, after grit blasting, is shown in figure 6. In all cases, coarse grit was used on side A and fine grit was used on side B. The fine grit increases s by more than an order of magnitude while reducing the correlation length. The distribution of the measured surface height before and after grit blasting aluminum plate Al-1 is shown in figure 7. The appearances of the fine and course grit-blasted surfaces are similar, however, the data indicates differently, with fine grit surface height being more widely distributed then the coarse grit.

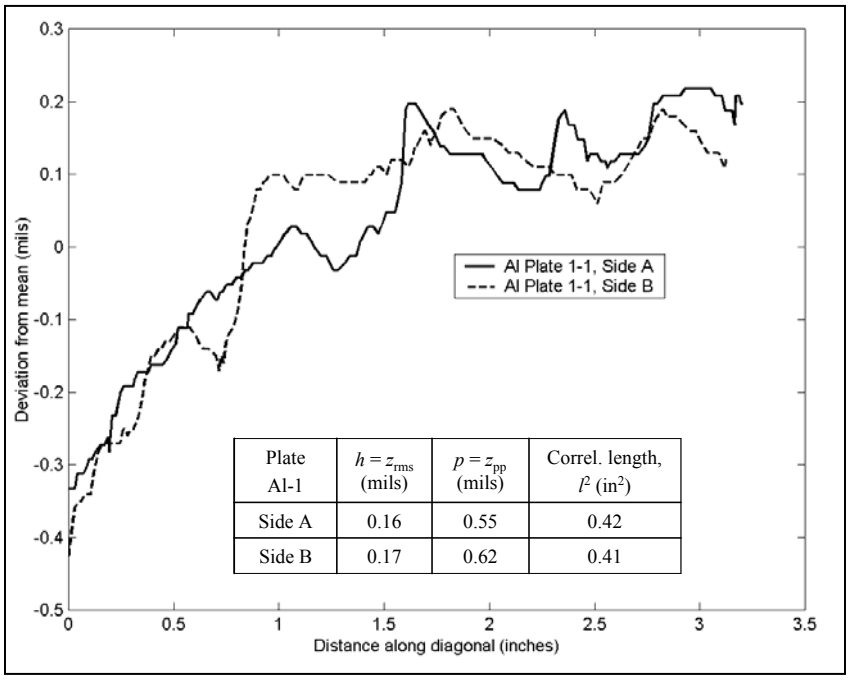

Plate Al-1	$h = z_{rms}$ (mils)	$p = z_{pp}$ (mils)	Correl. length, l^2 (in^2)
Side A	0.16	0.55	0.42
Side B	0.17	0.62	0.41

Figure 5. Measured surface roughness of plate Al-1 (smooth and highly polished).

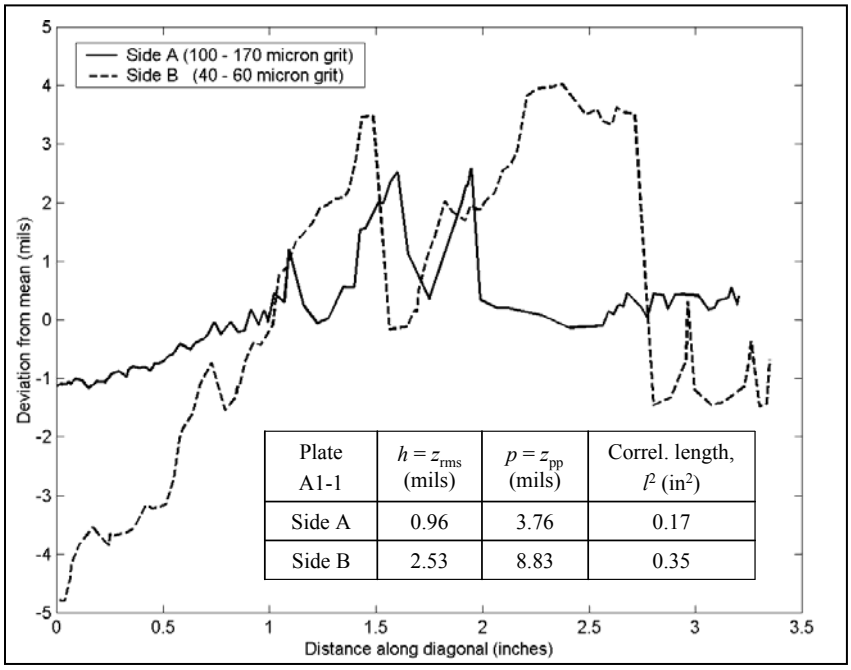

Plate A1-1	$h = z_{rms}$ (mils)	$p = z_{pp}$ (mils)	Correl. length, l^2 (in^2)
Side A	0.96	3.76	0.17
Side B	2.53	8.83	0.35

Figure 6. Measured surface roughness of plate Al-1 (after grit blasting).

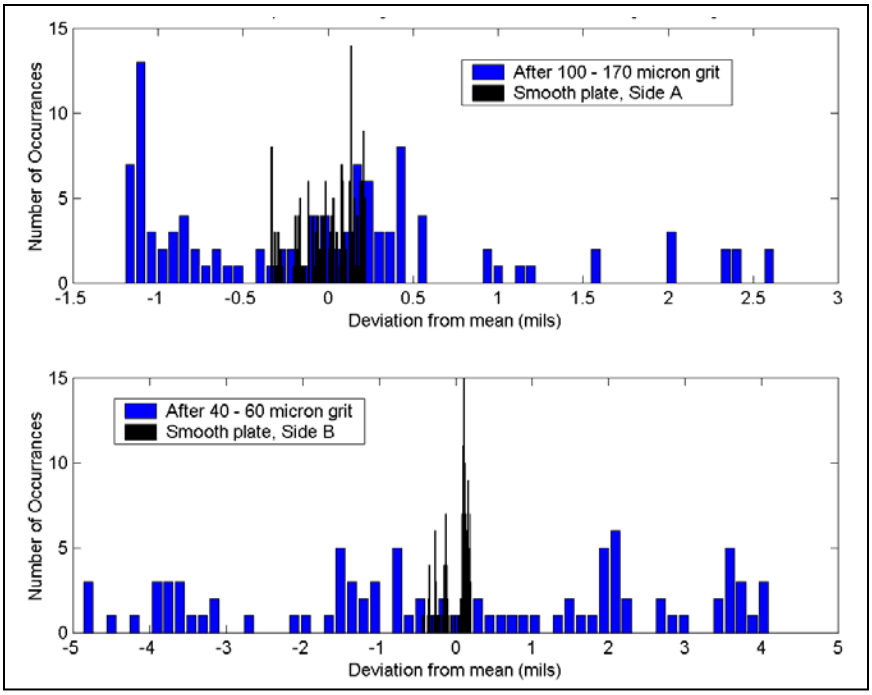

Figure 7. Measured surface height distribution of plate Al-1 before and after (a) course and (b) fine grit blasting.

3.5.2 RHA Plate Measurement Characteristics

The measured surface height for a large, heavily scaled and rusted RHA plate is shown in figure 8. The waviness can be apparent when traversing across 6-inches, so the two sides can have different height distributions. A measurement over small surface patches or smaller plates minimizes the effect of waviness. The results for small RHA plate 2-1 are shown in figure 9. This data provides a better characterization of the surface roughness. The rms height is more than an order of magnitude larger than the smooth aluminum plate. Although the RHA plate is not completely flat, the two sides appear more similar for a small plate with $s > 4$ mils. The distribution of the data for RHA plate 2-1 side A is shown in figure 10 compared to a Gaussian distribution having the same variance. We also include an exponential distribution, $\exp(-(z + s)/s)/s$, defined in the range $z = [-s, \infty]$, since this distribution is sometimes used to represent natural rough surfaces. The comparison for side B is shown in figure 11 and in all cases we use uniform bin sizes of 1 mil for the measured data. The appearance of these histograms can change depending on the bin size and number of data points, but we choose to use a consistent presentation of the data rather than adjust each histogram to more closely resemble a limiting distribution. We include only a single measurement in the histograms typically having 100 data points over the plate diagonal. Outlying data points are expected, but still the surface height appears to be approximately normally distributed, indicating a random variation.

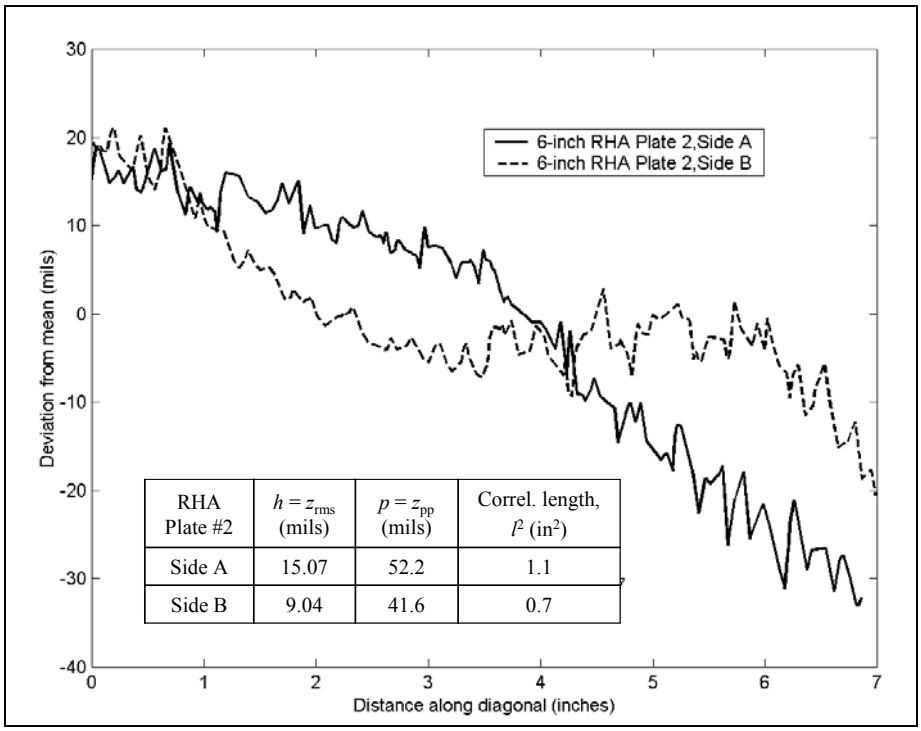

RHA Plate #2	$h = z_{rms}$ (mils)	$p = z_{pp}$ (mils)	Correl. length, l^2 (in^2)
Side A	15.07	52.2	1.1
Side B	9.04	41.6	0.7

Figure 8. Measured surface roughness of RHA plate 2.

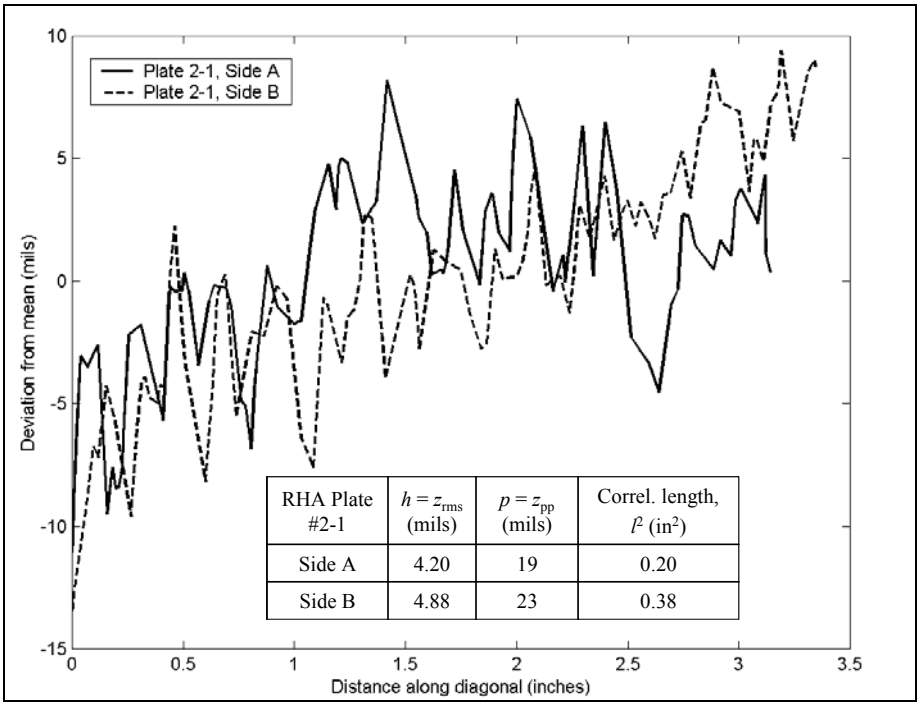

RHA Plate #2-1	$h = z_{rms}$ (mils)	$p = z_{pp}$ (mils)	Correl. length, l^2 (in^2)
Side A	4.20	19	0.20
Side B	4.88	23	0.38

Figure 9. Measured surface roughness of RHA plate 2-1.

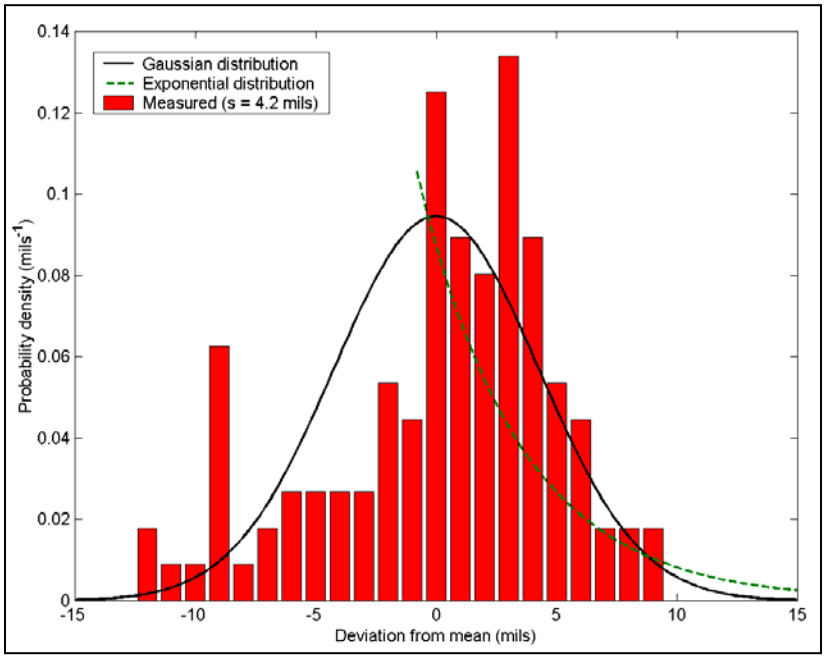

Figure 10. Measured surface height distribution of RHA plate 2-1, side A compared to Gaussian and exponential distributions.

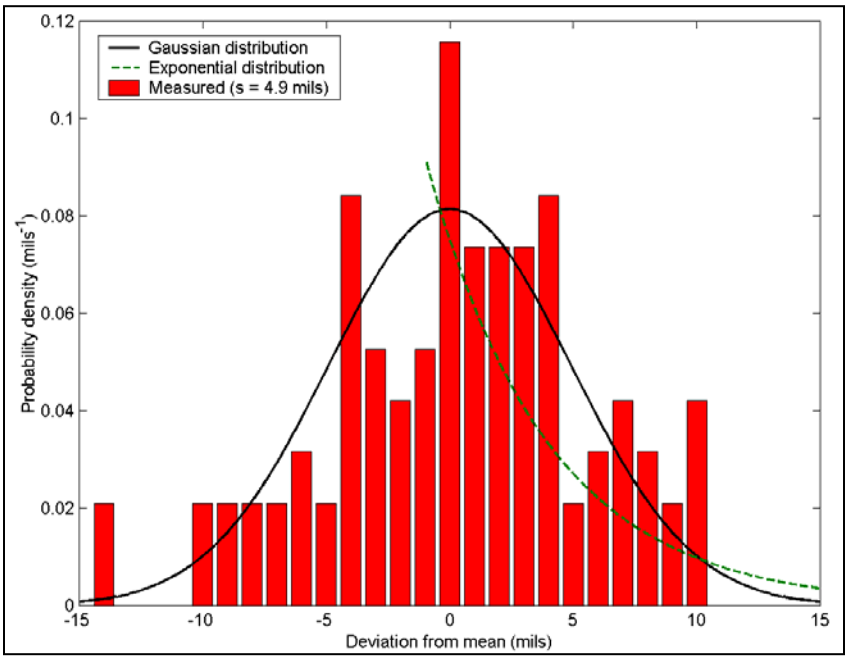

Figure 11. Measured surface height distribution of RHA 2-1, side B compared to Gaussian and exponential distributions.

3.5.3 RHA Plate 2-1 Measurement Characteristics after Grit Blasting

We show RHA plate 2-1 after grit blasting in figure 12 and compare the distribution of the data in figure 13 before and after grit blasting. For RHA plates, the grit blasting reduces *s* slightly, being more apparent with fine grit. The data compared to Gaussian and exponential distributions is shown in figure 14 and figure 15 for coarse and fine grit, respectively. After grit blasting the data appears slightly skewed. This can be an artifact of enforcing a zero mean condition on the measurements. This was not observed with the grit blasted aluminum plates. One could still argue that the height variation would approach a normal distribution, although grit blasting may have shifted the surface mean line slightly compared to the original plate.

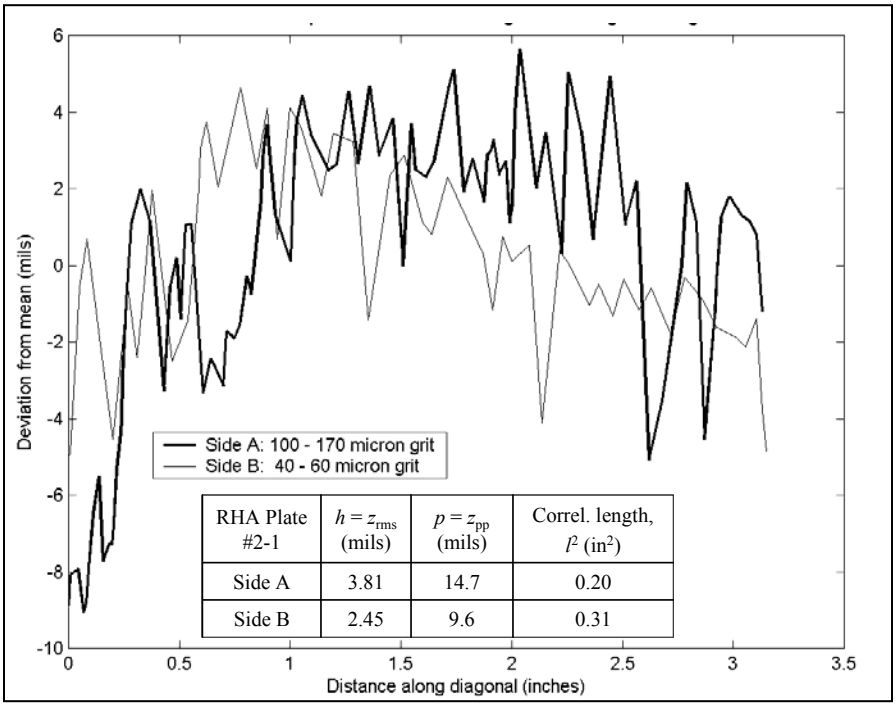

RHA Plate #2-1	$h = z_{rms}$ (mils)	$p = z_{pp}$ (mils)	Correl. length, l^2 (in^2)
Side A	3.81	14.7	0.20
Side B	2.45	9.6	0.31

Figure 12. Measured surface roughness of RHA plate 2-1 after grit blasting.

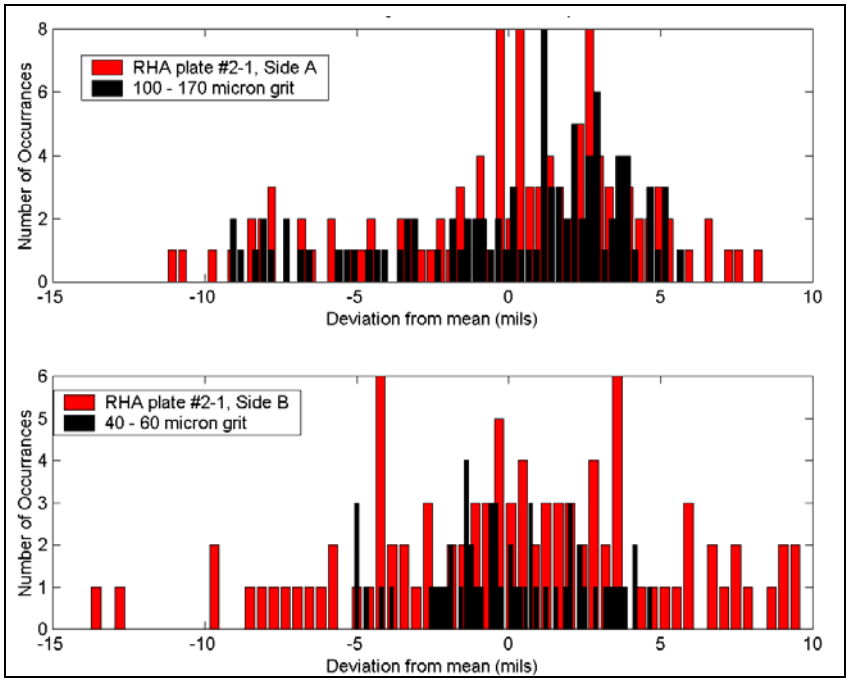

Figure 13. Measured surface height distribution of RHA plate 2-1 before and after (a) course and (b) fine grit blasting.

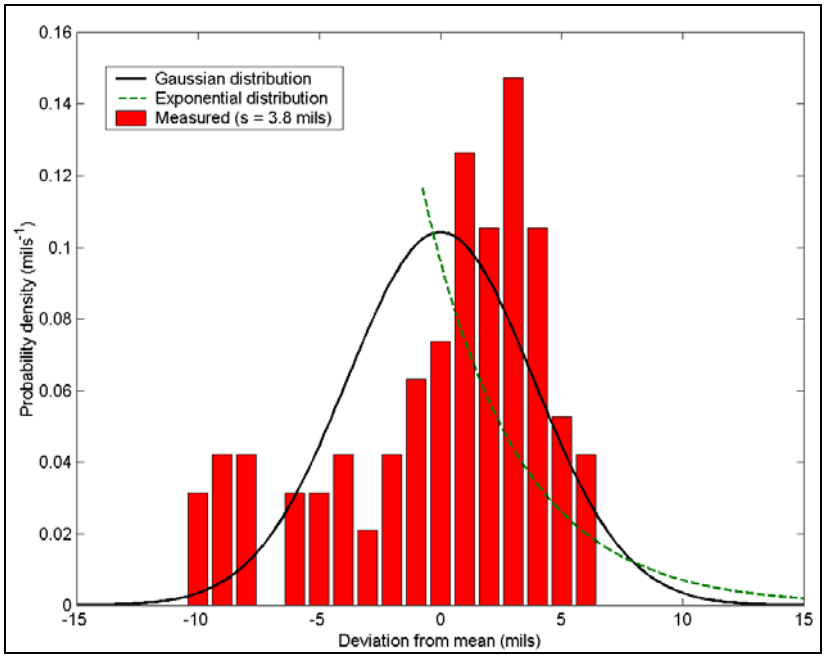

Figure 14. Measured surface height distribution of RHA plate 2-1, side A after course grit blasting compared to Gaussian and exponential distributions.

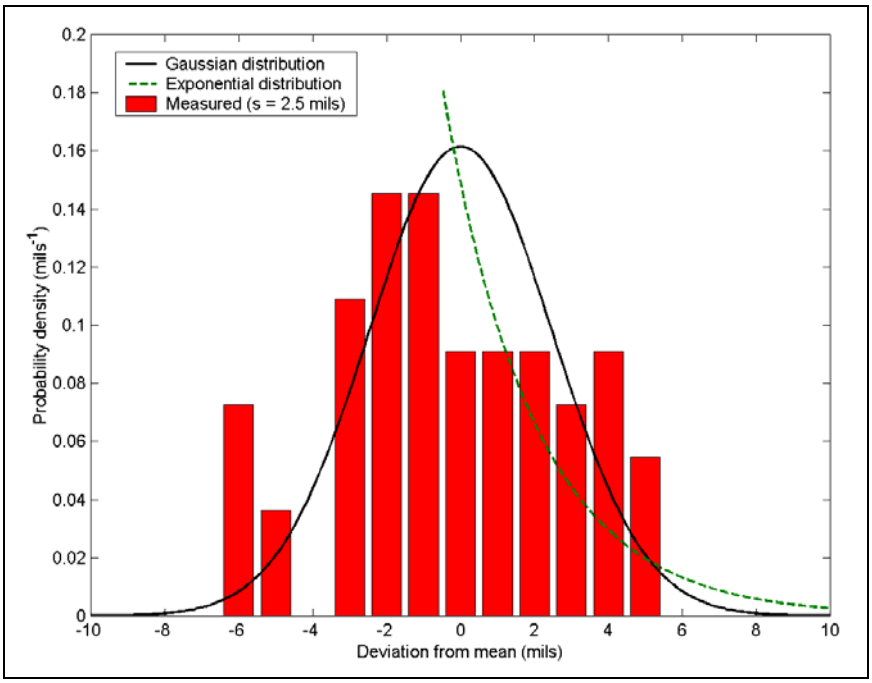

Figure 15. Measured surface height distribution of RHA plate 2-1, side B after fine grit blasting compared to Gaussian and exponential distributions.

3.5.4 RHA Plate 2-3 Measurement Characteristics after Grit Blasting

Another example of RHA plate measurements is shown in figure 16 for RHA plate 2-3 after grit blasting where side B appears to be bowed compared to side A. The distribution of the data is shown in figure 17 and figure 18 after blasting with coarse and fine grit, respectively. Similar results are obtained for other plates and, in general, the surface height variation appears random when traversing different paths with the Gage 2000R CMM. Thus, we use limiting distributions in our analysis with parameters determined from the statistics of the height measurements. The data is approximately normally distributed, being a better approximation than an exponential distribution. Still, it is not unusual for finished parts to have more peaks than deep pits so that in our analysis, we also consider an exponential distribution.

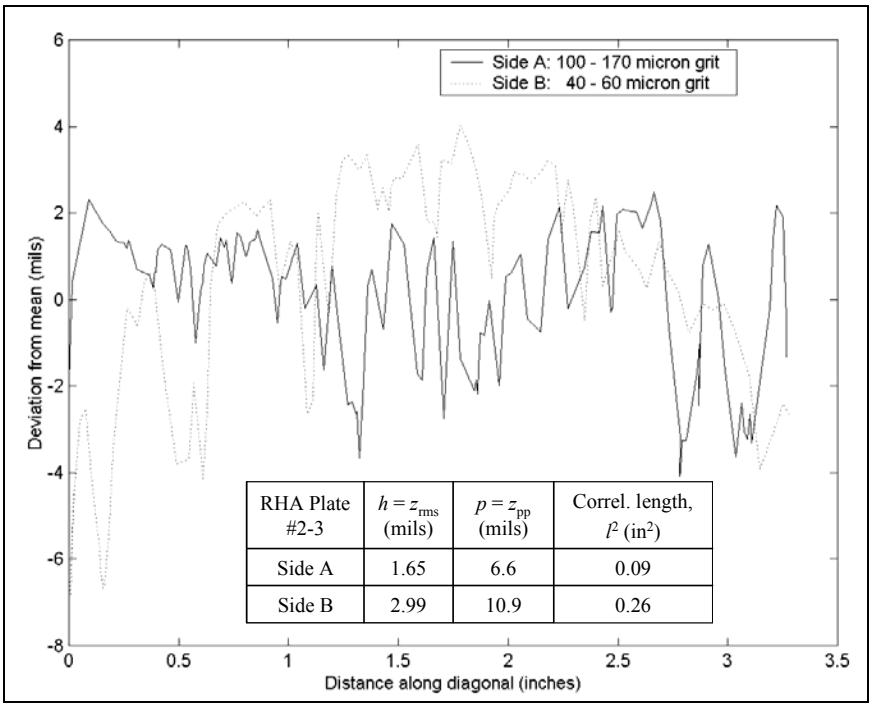

RHA Plate #2-3	$h = z_{rms}$ (mils)	$p = z_{pp}$ (mils)	Correl. length, l^2 (in^2)
Side A	1.65	6.6	0.09
Side B	2.99	10.9	0.26

Figure 16. Measured surface roughness of RHA plate 2-3 after grit blasting.

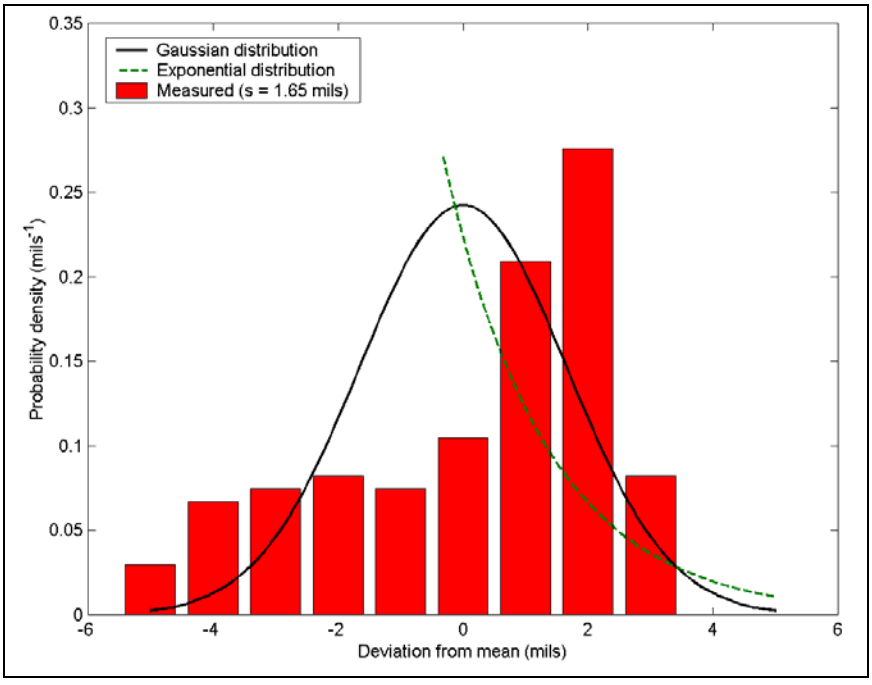

Figure 17. Measured surface height distribution of RHA plate 2-3, side A after course grit blasting compared to Gaussian and exponential distributions.

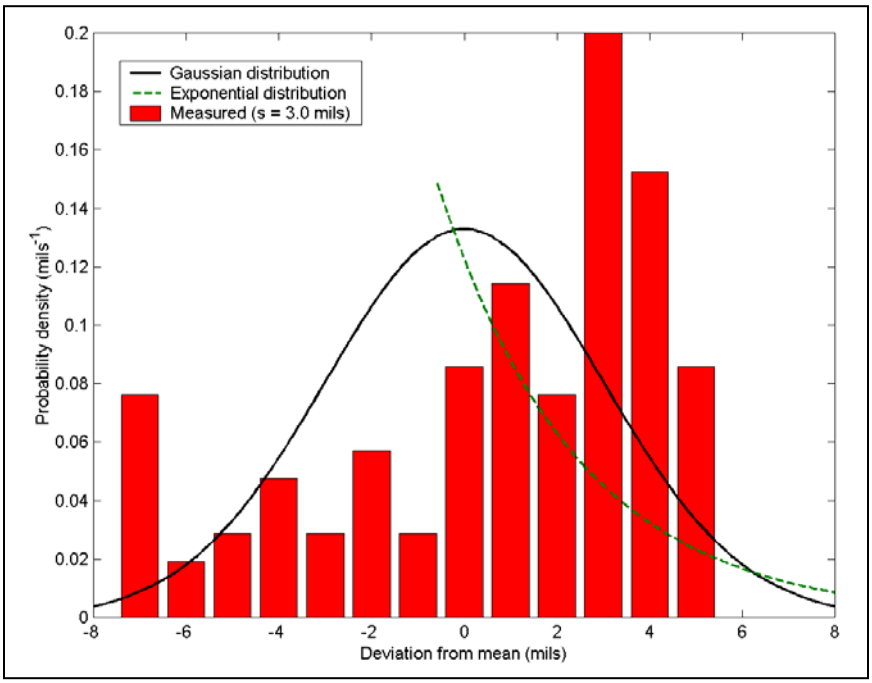

Figure 18. Measured surface height distribution of RHA plate 2-3, side B after fine grit blasting compared to Gaussian and exponential distributions.

3.5.5 RHA and Aluminum Plate Measurement Characteristics Summary

We measured the surface characteristics of the plates in the original condition and after modifying the surface with grit blasting. Table 3 summarizes the rms height, peak-to-valley height, $p = z_{pp}$, correlation length, l_c, and standard deviation for each of the graphs presented. We have shown that $s > 4$ mils for rusty RHA plates and that grit blasting reduces the standard deviation to $s \sim 2 - 3$ mils. There is a measurable difference when using different grit sizes, but it is small and either size is considered to represent the surface preparation for painting. Although grit blasting can alter the surface appearance, i.e., fine and course grit smooth the surface height distribution, the changes do not provide a large effect on the surface roughness. In our analysis we use the statistics obtained from the CMM data for each plate under consideration. All of the small RHA and aluminum plates had approximately Gaussian statistics and this remained true even after grit blasting.

Table 3. Summary of plate statistics.

Plate	Side	Grit Blasted	$h=z_{rms}$ (mils)	$p=z_{pp}$ (mils)	Correl. Length l_c^2 (in^2)	Stand Dev s (mils)
Al	A	No	1.39	5.2	1.3	-
Al	B	No	0.92	2.9	1.2	-
Al-1	A	No	0.16	0.55	0.42	-
Al-1	B	No	0.17	0.62	0.41	-
Al-1	A	Course Grit	0.96	3.76	0.17	-
Al-1	B	Fine Grit	2.53	8.83	0.35	-
RHA 2	A	No	15.07	52.2	1.1	-
RHA 2	B	No	9.04	41.6	0.7	-
RHA 2-1	A	No	4.20	19.0	0.20	4.2
RHA 2-1	B	No	4.88	23.0	0.38	4.9
RHA 2-1	A	Course Grit	3.81	14.7	0.20	3.8
RHA 2-1	B	Fine Grit	2.45	9.6	0.31	2.5
RHA 2-3	A	Course Grit	1.65	6.6	0.09	1.7
RHA 2-3	B	Fine Grit	2.99	10.9	0.26	3.0

3.5.6 Approximating Surface Condition Standard Deviation for Modeling

In general, we approximate very smooth metal by $s<1$ mil, but typical smooth metal parts with $s\sim1$ mil. For weathered surfaces, we would use $s\sim5$ mil although surface preparation could reduce this to $s<3$ mil. At millimeter wave (MMW) frequencies, these distinctions are not relevant, since even the roughest parts considered have $s<<\lambda$ and the effect on the plate backscatter is nearly negligible as we show in the next section. Of course, in a multi-bounce situation, such as corner returns, the reduction in the specular direction could be much larger and the effect on monostatic RCS may not be negligible.

4. Rough Surface Numerical Modeling

4.1 General

Modeling and theory are now examined to estimate the influence of surface condition, primarily random roughness and CARC, on RCS predictions. We begin our analysis by modeling a square plate with Xpatch using the surface roughness statistics presented in the previous section and then calculating the RCS at 34 GHz. Theoretical calculations using Gaussian and exponential surface distributions are considered and compared to small perturbation theory for slightly rough surfaces. The section concludes with an analysis to determine the impact of CARC on RCS.

The RCS of a smooth, flat surface can be calculated at high frequency using the PO approximation to the Stratton-Chu integral equation (*2-3*), which assumes a constant current in the radiation integral. This provides an accurate RCS pattern for angles near broadside. However, RCS patterns at angles near grazing are inaccurate because physical optics neglects polarization dependent effects and the effect of traveling wave returns (*3*). At intermediate angles, edge diffraction can become an important factor. This scattering mechanism is included in most RCS codes, although multiple interactions are typically neglected.

4.2. Modeling a Square Plate using Xpatch

For a numerical simulation, we use Xpatch with a faceted random rough surface created using Cifer, an Xpatch tool. We define a 3-inch square plate with 1000 nodes per edge and let Cifer generate a facet file with surface statistics based on the rms height and correlation length. An example is shown in figure 19(a) for s = 5 mil and l_c = 0.2 inch. The surface height ranges from z = -10 – 10 mils and the model is composed of 2 million triangular facets. For comparison, a plate having s= 5 mil with l_c = 2 inch is shown in figure 19(b) and has a much smoother appearance as expected. For l_c = 0.2 inch, but s = 50 mil, the plate is extremely rough as shown in figure 19(c).

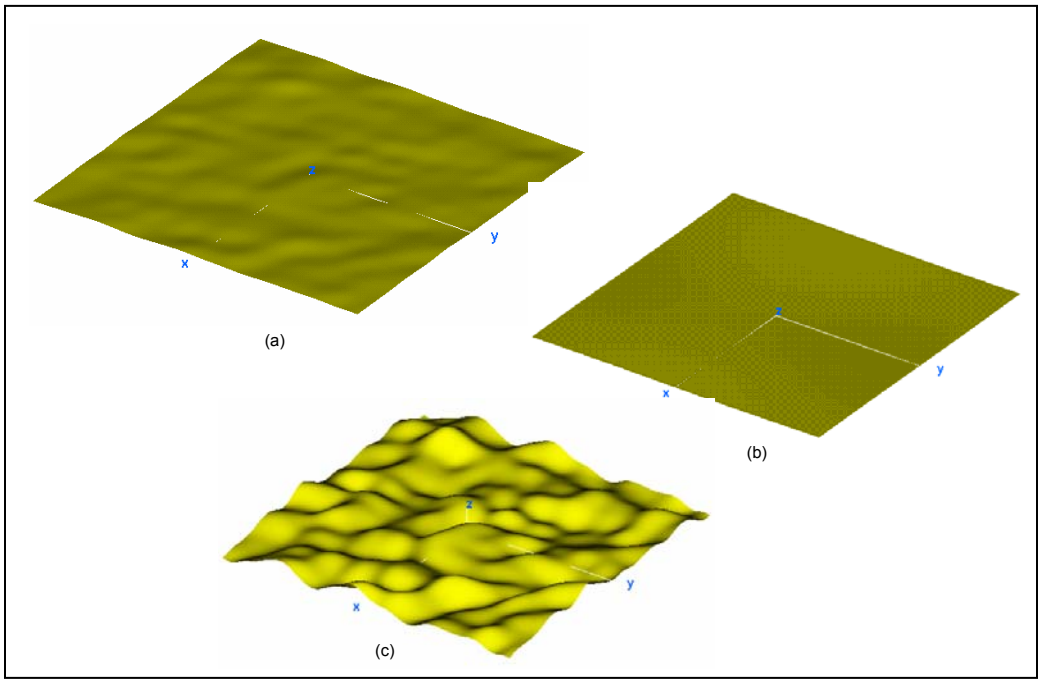

Figure 19. Xpatch facet models of a 3-inch square plate with faceted random rough surface having (a) h = 5 mils, l_c = 0.2 inch, (b) h = 5 mils, l_c = 2 inch, and (c) h = 50 mils, l_c = 0.2 inch.

4.3 Xpatch RCS Calculations for the Modeled Square Plate

The monostatic RCS pattern near broadside at 34 GHz is shown in figure 20 for s = 0, 5, and 50 mil all with l_c = 0.2 inch. As expected the effect of s = 5 mil is almost negligible, but s = 50 mil significantly reduces the RCS. Notice that the pattern is no longer symmetric around broadside and for s = 50 mil the RCS at $\theta = \pm 10^o$ increases indicating alignment with a local tangent plane at this incident angle. This result is for a single realization of a random surface. However, many realizations would normally be used to determine the distribution of the predicted RCS. RCS data based on these plates would correspond to specific realizations, making it impossible to create an exact facet model representing all of the given plates. Thus, the effect of roughness must be addressed in a statistical sense. One can only estimate the RCS corresponding to a large number of measurements on plates having equal surface roughness statistics.

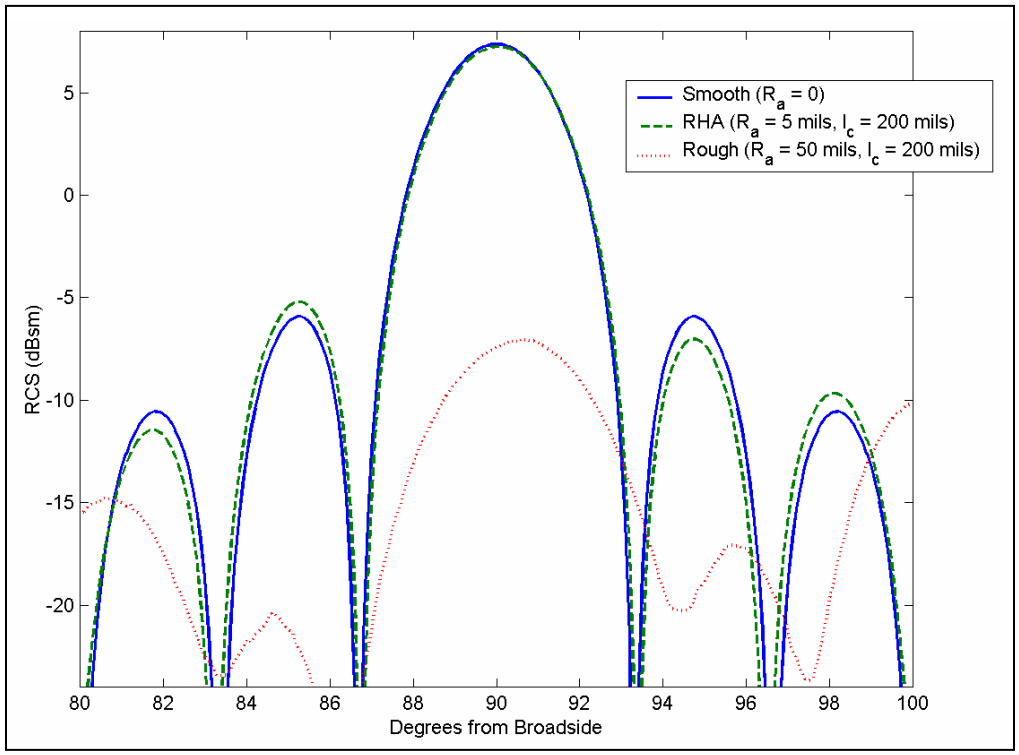

Figure 20. Xpatch results for Gaussian roughness similar to RHA plate 2-1, side A at 34 GHz with faceted rough surface as a function of roughness height.

5. Theoretical Calculations

5.1 General

The scattering of EM waves from rough surfaces has been widely studied with much of the theory developed for irregularities large compared to wavelength. In this case, Kirchoff's theory applies so that a tangent plane can be defined at every point on the surface for calculating the local fields. For small irregularities perturbation techniques are more appropriate and natural surfaces have roughness superimposed on larger undulations (*4-6*). For the small plates considered here, we neglect the large scale waviness, and the roughness is small compared to the wavelengths of interest. The surface height, z, is considered to be random and is often characterized in terms of the Rayleigh parameter

$$\sqrt{g} = ks\left(\cos\theta + \cos\theta_s\right) \tag{1}$$

where k is the wavenumber, θ and θ_s are the incident and scattered angles from broadside, respectively. Our height distributions have zero mean so that $h = s$ is the rms surface height and for backscatter $g = (2kh\cos\theta)^2$ (*7*).

5.1.1 Modified PO Model RCS Calculations for a Square Plate

In the specular direction, the effect of moderate roughness is well described by the modified PO model in which the RCS is simply reduced by e^{-g} compared to the smooth surface (*7-9*). The Xpatch results indicate a larger effect of surface roughness on the RCS pattern compared to the modified PO model (equation 1) as shown in figure 21. The RCS is at 34 GHz with s = 5 mils and l_c = 0.2 inch, which most closely approximates RHA Plate 2-1, side A. This is expected since equation 1 is the average effect whereas Xpatch is for a specific surface as evident by the asymmetric RCS pattern.

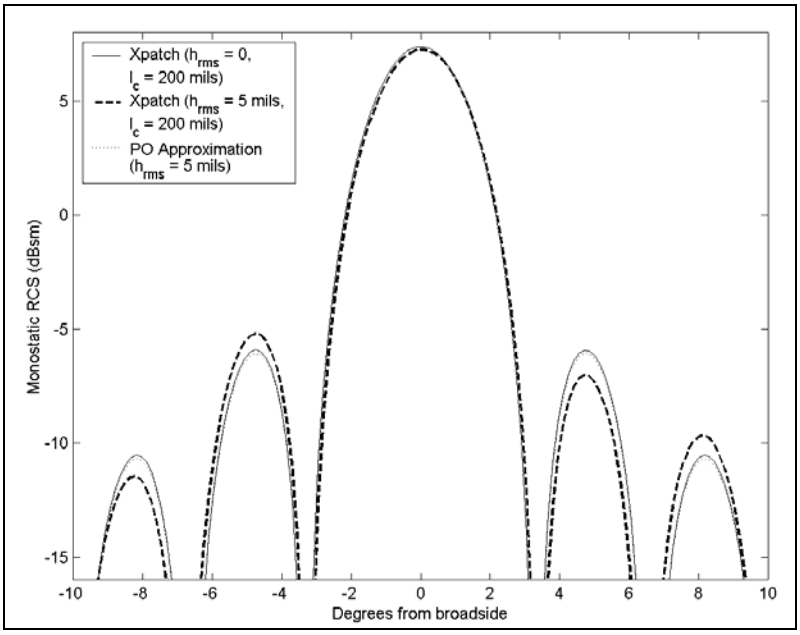

Figure 21. Xpatch results for Gaussian roughness similar to RHA plate 2-1, side A, at 34 GHz compared to Modified PO Model.

We showed that the RHA plates have an rms roughness $h < 5$ mils and this has an almost negligible effect on the specular scattering, as shown in figure 22, over a wide frequency range. The effect of surface condition on W-Band RCS is larger and may not be negligible, so a similar investigation at W-Band frequencies is recommended.

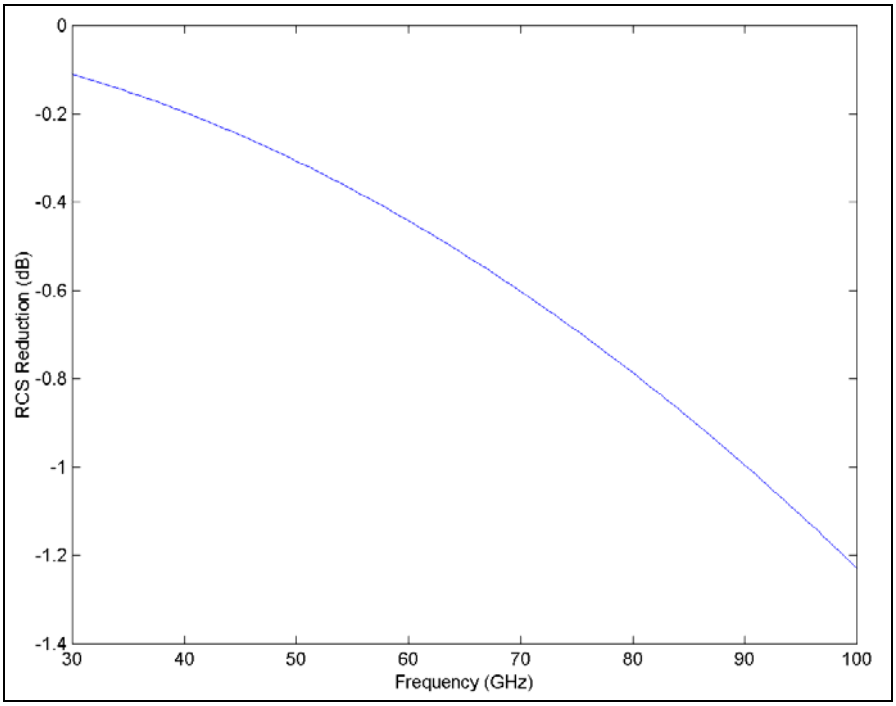

Figure 22. The effect of surface roughness with $h = s = 5$ mils on the broadside return of a perfectly conducting square plate.

We desire a similar theory that can be used to estimate the effect of random roughness on the monostatic RCS pattern. High frequency approximations can be readily applied to a random surface distribution typically assumed to be Gaussian, although this is not required (*7*). In many cases the scattering theory is formulated for large roughness, where shadowing can become important at some incident angles (*8-13*).

5.1.2 Effect of Roughness on Monostatic RCS Pattern

For a moderately rough surface ($ks \sim 1$), Gaussian statistics can be assumed with the actual surface height distribution becoming more important with increasing roughness (*10-12*). Our measurements of the surface height represent a single realization of the random surface (i.e., along a specific path) and many of these measurements would produce a distribution closer to Gaussian. However, a single realization tends to be skewed toward positive excursions from the mean line when the surface has more ridges than deep pits. The opposite might be apparent for an extremely pitted surface (e.g., poorly cast parts) which would skew the distribution toward negative excursions. The measured surface height can appear to be exponentially distributed as previously shown, so that this type of distribution is also of interest. For backscatter, the incident direction is directly related to the local surface slope, $z' = \tan\theta$, also having zero mean, so the standard deviation of the derivative distribution, s_s, is the rms slope, h_s. The backscatter depends on the probability that the surface slopes have the proper orientation and can be written in terms

of the surface correlation function. The correlation function is assumed to be Gaussian with correlation length, l_c. Beckman uses a series approximation appropriate for small spatial wavenumber increments, $\tau = \zeta - \zeta'$,

$$R(\tau) = \exp\left(-\frac{\tau^2}{l_c^{\,2}}\right) = 1 - \frac{s_s^2}{2s^2}\tau^2 + \mathrm{O}(\tau^4) \tag{2}$$

Then the scattered field can be written in terms of s_s which we calculate from the derivative of the measured surface height. The effect of the surface roughness is quantified by the backscattered power normalized to that at broadside (*7*)

$$\frac{W(\theta)}{W(0)} = \frac{1}{\cos^2\theta}\exp\left(-\frac{\tan^2\theta}{2s_s^{\,2}}\right) \tag{3}$$

for Gaussian statistics, and

$$\frac{W(\theta)}{W(0)} = \frac{1}{\cos^2\theta}\exp\left(-\frac{|\tan\theta|}{s_s}\right) \tag{4}$$

for an exponential surface height distribution. These expressions are derived using geometrical optics (GO) in the limit of vanishing wavelength. But, at fixed frequency, this assumption actually corresponds to large roughness, $ks >> 1$, so are less appropriate for the slightly rough plates ($ks < 0.1$) used in this investigation. We also use the theory of Eom and Fung for near broadside backscatter. Although the numerical calculations do not rely on GO, the derivation is subject to Kirchoff's approximation (often called the tangent plane approximation) which assumes large roughness. We show results using this theory, since they are slightly different than that obtained using equation 3. For Gaussian surfaces and correlation function, $R(\tau)$, the PEC backscatter coefficient is independent of polarization (*4*)

$$\sigma(\theta) = 2k^2\cos^2\theta e^{-g}\sum_1^\infty \frac{g^n}{n!}\frac{l_c^2}{2n}\exp\left(-\frac{(2kl_c\sin\theta)^2}{4n}\right) \tag{5}$$

The series converges rapidly for small g and we normalize the result to the RCS of a smooth plane. We obtain s and l_c from the measured surface height and take a numerical derivative to calculate s_s.

5.1.2.1 Comparing Normal and Exponential Surface Distributions at K_a-Band

We compare the monostatic RCS at 34 GHz of a smooth plate to that obtained from equations 3 and 5 for a normal surface and to that obtained from equation (4) for an exponential surface distribution. The comparison is shown in figure 23 for RHA plate 2-1, side A, indicating slight differences between different approximations for the normal surface height distributions. There is also some difference between the normal and exponential distributions, although these differences would be difficult to measure in near specular directions. For the slightly rough plates considered here the specular return is unaffected since $ks < 0.1$ (see figure 22). The

comparison for RHA plate 2-1, side B is shown in figure 24, where, for these parameters the results from equations 3 and 5 are the same for normal surface height distributions. The theoretical differences depend on approximations for the correlation function with equation 5 being more sensitive to the correlation length. After grit blasting both the rms height and slope are reduced with a smaller correlation length.

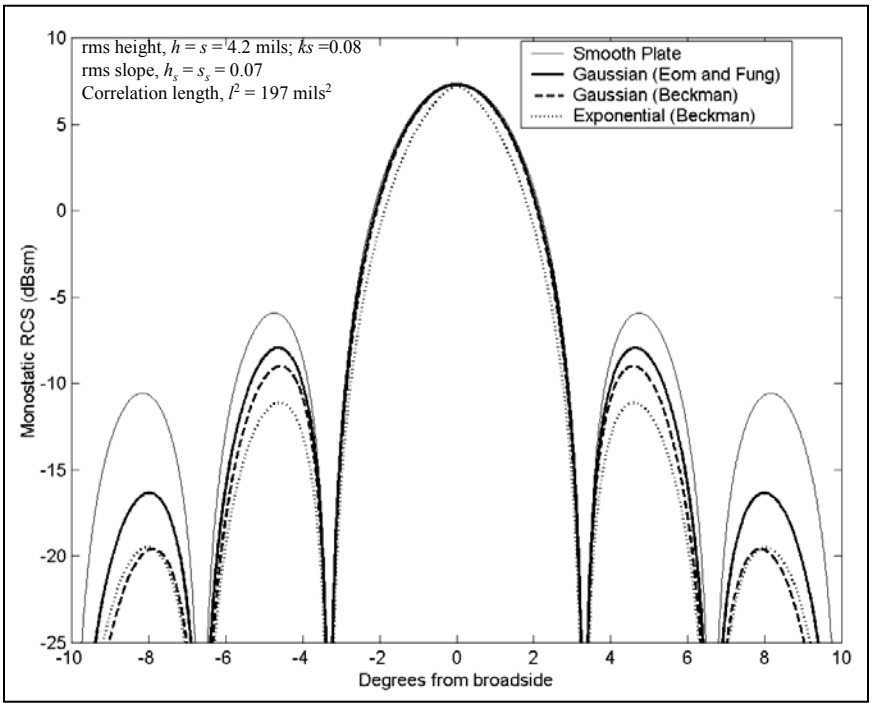

Figure 23. Effect of surface roughness on RCS for the statistics of RHA plate 2-1, side A at 34 GHz.

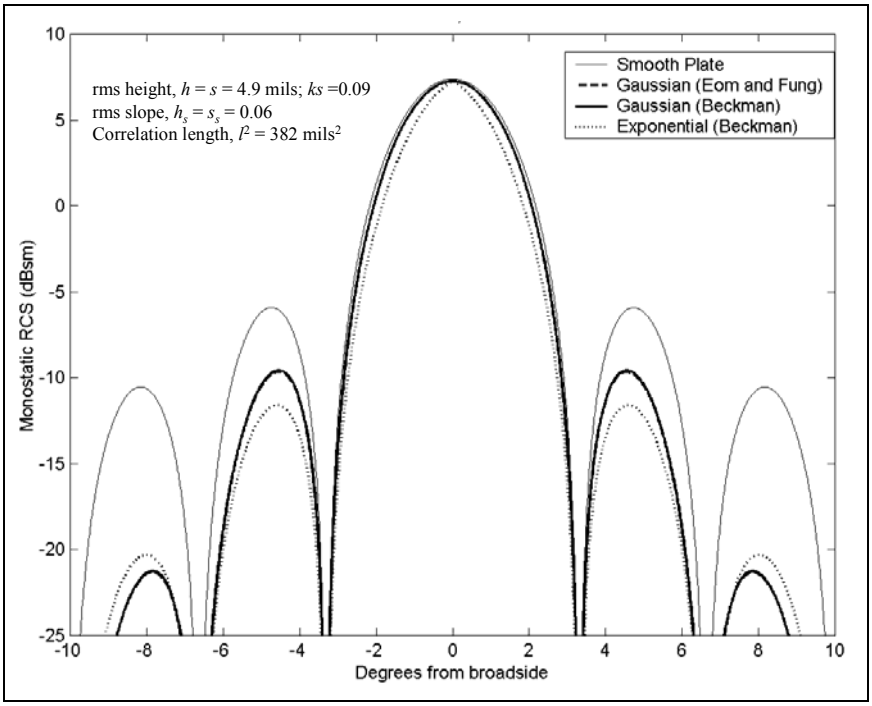

Figure 24. Effect of surface roughness on RCS for the statistics of RHA plate 2-1, side B at 34 GHz.

After course grit blasting, the roughness is about half that of the original plate. The calculated RCS reduction for grit-blasted RHA plate 2-3, side A is shown in figure 25. Beckman's result shows a larger effect on the monostatic return for lower rms slope whereas the result from equation 5 is only a slight effect since the correlation length is much smaller. After fine grit blasting, the roughness is about half that of the original plate. The calculated RCS reduction for grit-blasted RHA plate 2-3, side B is shown in figure 26. The rms slope is even lower, so Beckman's result shows a larger effect on the monostatic return. For side B the result from equation 5 is a larger effect since the correlation length is larger than that for side A.

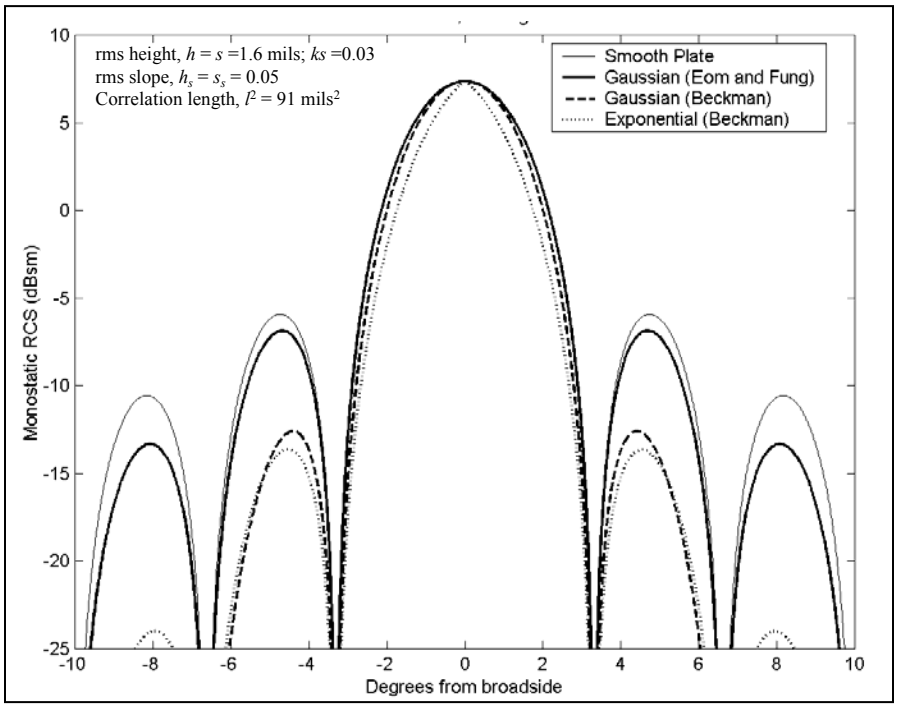

Figure 25. Effect of surface roughness on RCS for the statistics of RHA plate 2-3, side A after coarse grit blasting at 34 GHz.

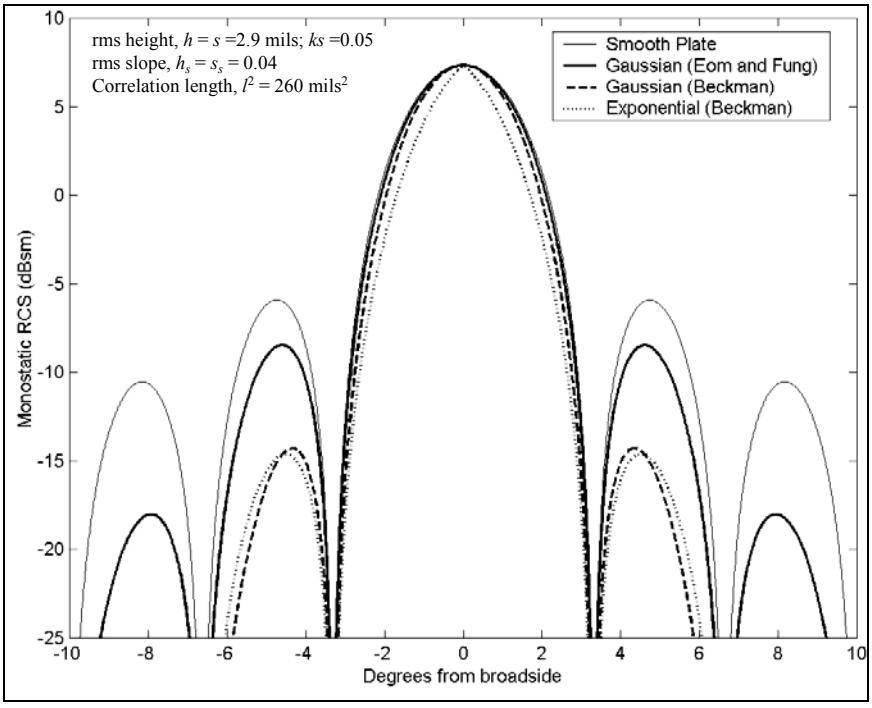

Figure 26. Effect of surface roughness on RCS for the statistics of RHA plate 2-3, side B after fine grit blasting at 34 GHz.

5.1.2.2 Small Perturbation Theory

At K_a-Band, the effect of surface roughness is small on the monostatic RCS and would not be an observable influence in the data collected on these plates at most RCS measurement facilities. The effect on the monostatic RCS pattern from equations 3–5 probably overestimates the effect for slightly rough surfaces. This is because of the GO approximation, which would strictly apply only for very rough surfaces or extremely high frequencies. Using equation 5 also appears restricted to larger roughness, since the local tangent plane is assumed larger than the wavelength. At K_a-Band frequencies this is not true for the plates considered here, so one would use small perturbation theory to describe the effect of slight roughness on the plate backscatter. The first order perturbation on the PO fields can be determined assuming Gaussian surface statistics (*10-13*). The perturbation term depends on the surface statistics through the two-dimensional spectral power density function,

$$S(k_{sx},k_{sy}) = \frac{s^2}{(2\pi)^2}\int_{-\infty}^{\infty}\int_{-\infty}^{\infty} R(\tau)\exp(i\xi\tau)R(\tau')\exp(i\xi\tau')d\tau d\tau' = \frac{s^2}{(2\pi)^2}\left[\int_{-\infty}^{\infty} R(\tau)\exp(i\xi\tau)d\tau\right]^2 \tag{6}$$

since the surface properties in each direction are assumed Gaussian and independent. The backscattering cross section per unit area is the superposition of that for the smooth surface, $[\sigma_{pp'}(\theta, \phi)]_0$, and a small fluctuation when $4k^2s^2 << 1$ written as (*10*)

$$\left[\sigma_{pp'}(\theta,\phi)\right]_1 = 8k^4\Gamma_{pp'}S^2(-2k\sin\theta\cos\phi, -2k\sin\theta\sin\phi) \tag{7}$$

where p and p' are the transmitted and received polarization, respectively and

$$\Gamma_{pp'} = \begin{cases} 0 & \text{for cross-polarization} \\ \cos^4\theta & \text{for HH-polarization} \\ (1+\sin^2\theta)^2 & \text{for VV-polarization} \end{cases} \tag{8}$$

Numerical results should be obtained using a Gaussian correlation function since the measured surface height represents only a single realization of the random surface. This is not shown here, since for our parameters it is obvious that the perturbation term is small compared to the GO contribution which is (per unit area)

$$\left[\sigma_{pp'}\right]_0 = \pi\delta_{pp'}\delta(\sin\theta\cos\phi)\delta(\sin\theta\sin\phi) \tag{9}$$

For backscatter in the plane of incidence there is no polarization dependence and the surface height perturbations contribute to the backscatter even at normal incidence, as discussed by Brown (*10*). Similar to his example, our typical parameters are ks~0.01 for aluminum plates and ks~0.1 for RHA plates. Both have correlation length about three times the wavelength, and the perturbation term is more than 15 dB less than the smooth surface backscatter at normal incidence. The perturbation theory approach fails when the contribution approaches that of the smooth surface, in which case the previous approximations are more appropriate as mentioned by Brown (*10*). The small scale random roughness would have only a small effect on the RCS

and the large scale roughness (waviness) would dominate the influence of the irregular surface compared to a smooth plate. For small plates, the large scale roughness is assumed negligible, so for our parameters the effect on RCS is small and less than typical measurement uncertainties.

5.1.2.3 Measured RCS Patterns Using a K_a-Band Monopulse Radar

An example of some measured RCS patterns are shown in figure 27 using a K_a-Band monopulse radar with 1.6 GHz bandwidth (*14*). These results are frequency averaged RCS for Vertical-Vertical polarization measured for an aluminum plate compared to the front and back of RHA plate 2-3. The effect of roughness at K_a-Band is most evident in the non-symmetric variation in the RCS pattern, but the amplitude variations are inconclusive. Amplitude uncertainty due to repeating the target's position was not determined for this investigation. However, measurement uncertainty of ±1 dB has been demonstrated on targets with lower RCS and more rigorous alignment constraints (*15*). It is expected that the uncertainty in amplitude of the reported measurements is at least as good as this and more likely better. A better controlled experiment is planned in order to improve the measurement repeatability for a set of plates having different surface characteristics. Based on our analysis, the measurement accuracy desired for the RHA plates is difficult to obtain, but under controlled conditions we hope to demonstrate a repeatability for monostatic RCS less than 0.25 dB.

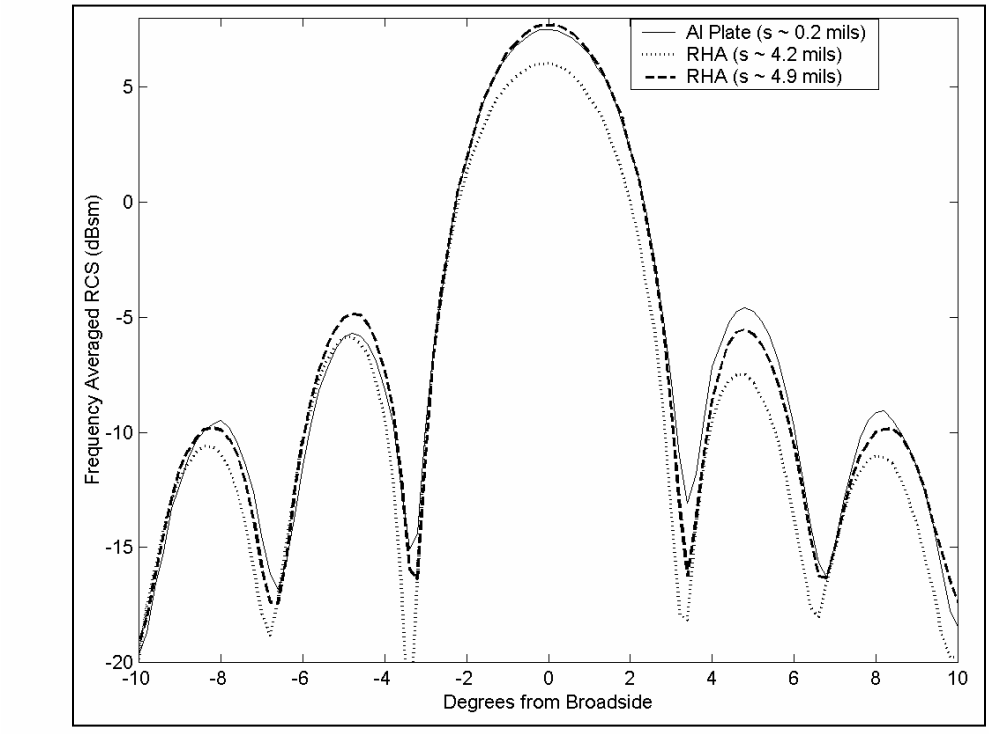

Figure 27. Measured RCS patterns.

5.2 Thin Coatings Analysis

The final objective of this experiment was to estimate the influence of surface condition, primarily a plate with random roughness and a coating of CARC on RCS predictions. The small aluminum plate and two small RHA plates were painted by the ARL Weapons and Materials Research Directorate (WMRD) using standard application procedures. The plates were painted with CARC primer (MIL-P-53030) on side A and CARC green paint (MIL-DTL-64159) on side B.

Standard coatings are on the order of 3-mils thick (*16*). We assumed 2 coats of paint and 4 coats of primer to obtain good coverage on the plates. We used an approximate thickness, $d_1 = 0.4$ mm for the primer layer and an approximate thickness, $d_2 = 0.2$ mm for the green CARC layer. The relative permittivity of commercial paints[8] was provided as $\varepsilon_r = 4.2 - j0.02$, with a relative permeability, $\mu_r = 1$. This would imply that such thin coatings would have a negligible effect on RCS and would be difficult to measure at K_a-Band frequencies. The Military Specification for coatings are reported to have somewhat larger loss with the imaginary part of the permittivity less than about 0.1 ± 5% (*16*). For the primer layer we use $\varepsilon_r = 6 - j0.1$, while for the CARC top coat we use $\varepsilon_r = 3.4 - j0.1$, both with relative permeability, $\mu_r = 1$ (*16*).

For a uniform coating of thickness d, with normalized admittance, $y_1 = (\varepsilon_r/\mu_r)^{1/2}$, the reflection coefficient at normal incidence can be written (*2*)

$$R = \frac{\tanh(-ik_1 d) - y_1}{\tanh(-ik_1 d) + y_1} \tag{10}$$

with $k_1 = k_0(\varepsilon_r\mu_r)^{1/2}$, the wavenumber of the coating. There are published experimental results that indicate a coating with $\varepsilon_r = 2.53 - j0.145$, having $d = \lambda/20$ can reduce the broadside return by 5 dB (*17*). We have not been able to reproduce those results even for thicknesses approaching a wavelength (*18*). Using equation 10 one would only expect a negligible effect (~0.03 dB) for such a thin coating. For multi-layer systems we use a recursion relation based on equation 10 assuming the coatings are applied to a base metal. The specular reduction for arbitrary layers of uniform coatings compared to a bare plate can be calculated similarly. The influence of thin, low-loss dielectric coatings on RCS would be difficult to measure at K_a-Band frequencies for the parameters considered here.

The specular reflected power, as a function of incidence angle, is shown in figure 28 at a frequency of 34 GHz, where the total thickness $d = 0.6$ mm ~ $\lambda/15$. This result implies that typical CARC treatments would have a negligible effect (< 0.1 dB) on the broadside RCS. A much thicker coating or larger dielectric (or magnetic) dissipation would be required to significantly reduce the return of a metal target. The broadside RCS reduction for these coatings applied to a metal plate is shown in figure 29 as a function of frequency. The combination of the primer and CARC paint reduces the specular reflection somewhat more than the individual

[8] Damaskos, Inc. Concordville, PA (http://www.damaskosinc.com/).

layers at K_a-Band. For a numerical example with Xpatch we chose a single layer coating with $\varepsilon_r = 4.2 - j0.1$ and 0.6 mm (24 mil) thickness. We apply this coating to a smooth and rough plate and compare the Xpatch results for the RCS pattern in figure 30. The RCS reduction at K_a-Band owing to the coating is on the same order as that due to diffuse scattering with the combined effect being about 0.2 dB. For the electrical parameters used here, the CARC paint or primer coatings on our plates would have a negligible effect on the RCS pattern at K_a-Band.

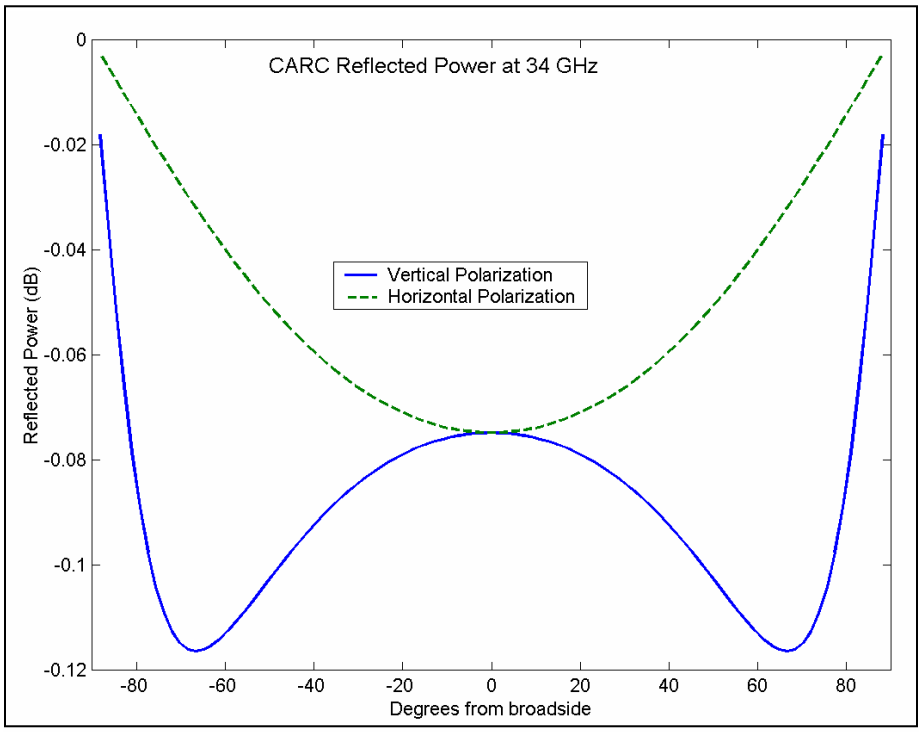

Figure 28. The effect of CARC on the specular reflection of a flat plate at 34 GHz versus incidence angle.

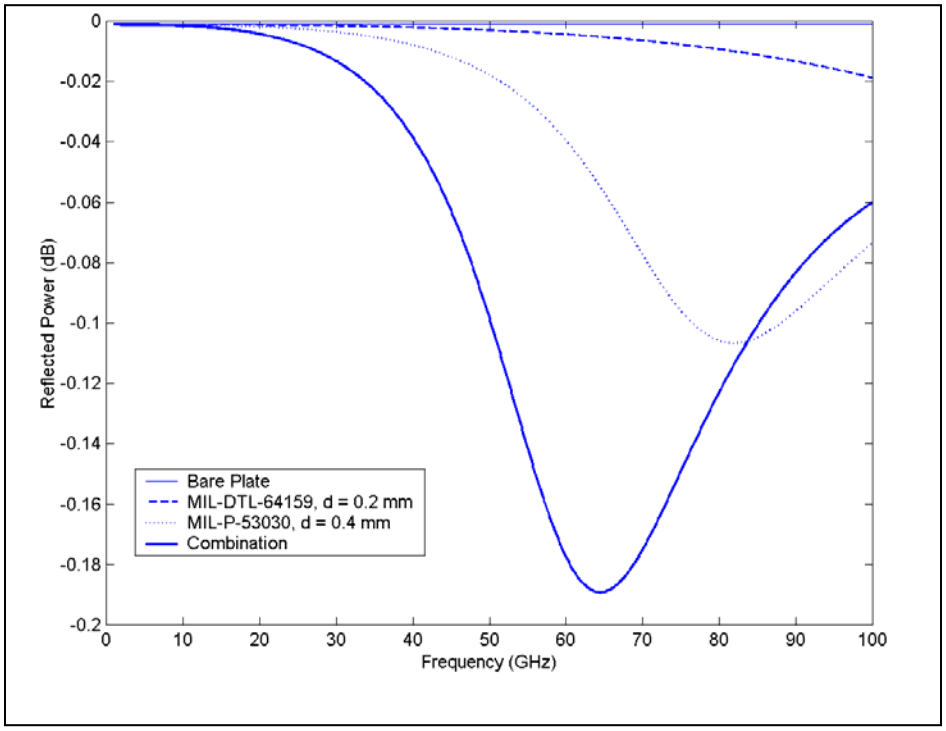

Figure 29. Effect of lossy dielectric coating on broadside reflectivity of flat plate versus frequency.

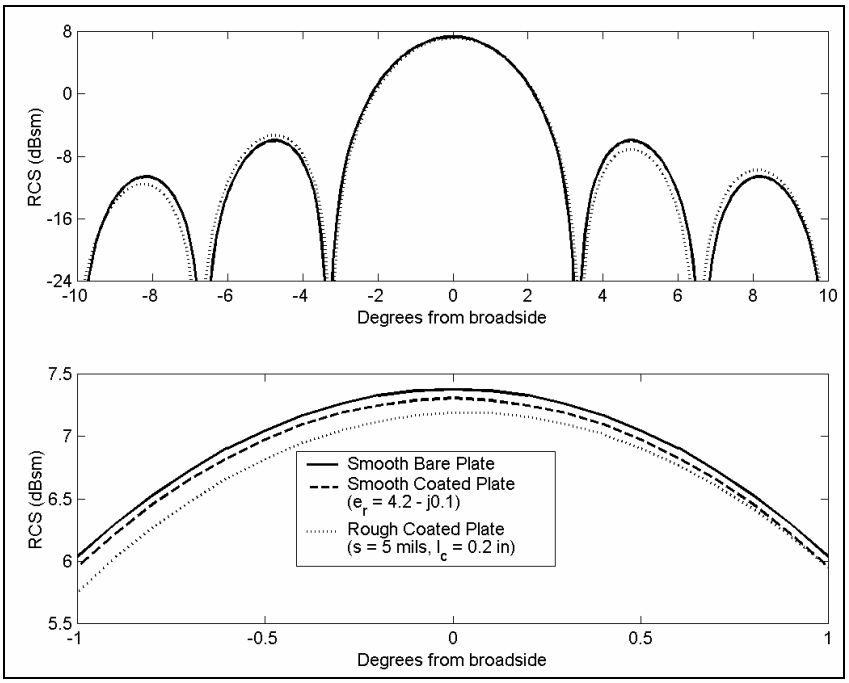

Figure 30. Xpatch results for Gaussian roughness similar to RHA plate 2-1, side A at 34 GHz with faceted rough surface and a single CARC layer.

6. Conclusions

The standard deviation of the height for a small aluminum plate was found to be approximately 0.2 mils (refer to paragraph 3.5.1).

Plate statistics blasted with fine grit are more widely distributed as compared to plates blasted with coarse grit (refer to paragraph 3.5.1).

The rms height of the rusted RHA plate is more than an order of magnitude larger than the rms height of the smooth aluminum plate (refer to paragraph 3.5.2).

We showed the standard deviation of the height for rusted RHA plates is greater than 4 mils and grit blasting reduces the standard deviation to approximately 2-3 mils (refer to paragraph 3.5.5).

There is a measurable difference when using different grit sizes, but it is small and either size is considered to represent surface preparation for painting (refer to paragraph 3.5.5).

The small aluminum and RHA plates had approximately Gaussian statistics before and after grit blasting (refer to paragraph 3.5.5).

In general, the height standard deviation of smooth metal can be approximated as less than a mil, while typical smooth metal parts can be approximated as 1 mil. For weathered RHA surfaces, the standard deviation could be approximated as 5 mils, although if the surface has been prepared, a standard deviation of less than 3 mils would not be unreasonable (refer to paragraph 3.5.6).

At K_a-Band the effect of surface roughness is small on the monostatic RCS and would not have an observable influence on data collected at most RCS measurement facilities (refer to paragraph 5.1.2.2).

Typical CARC treatments would have a negligible effect (<1 dB) on the broadside RCS. A much thicker coating or larger dielectric (or magnetic) dissipation would be required to significantly reduce the return of a metal target (refer to paragraph 5.2)

7. Recommendations

Based on our analysis, the measurement accuracy desired for the RHA plates is difficult to obtain, but under controlled conditions, we hope to demonstrate a repeatability for monostatic RCS less than 0.25 dB (refer to paragraph 5.1.2.3)

The effect of surface condition on W-Band RCS is larger than at K_a-Band and may not be negligible, so a similar investigation at W-Band frequencies is recommended (refer to paragraph 5.1.1).

8. References

1. Andersh, D. J., et. al., Xpatch: A High Frequency Electromagnetic Scattering Prediction Code and Environment for Three-Dimensional Objects. *IEEE Transactions on Antennas and Propagation*, **February 1994**, *36*, 65–69.

2. Knott, E. F.; Shaeffer, J. F.; Tuley, M. T. *Radar Cross Section*; Artech House: Norwood, Mass., 1985.

3. Knott, E. F. *Radar Cross Section Measurements*, 2nd Edition; Van Nostrand Reinhold: New York, 1993.

4. Eom H. J.; Fung, A. K. A Comparison between Backscattering Coefficients Using Gaussian and Non-Gaussian Surface Statistics. *IEEE Trans. on Ant. and Prop.* **July 1983**, *31* (4), 635–638.

5. Fung, A. K.; Chan, H. Backscattering of Waves by Composite Rough Surfaces. *IEEE Trans. on Ant. and Prop.* **September 1969**, *17* (5), 590–597.

6. De Roo, R. D.; Ulaby, F. T. Bistatic specular scattering from rough dielectric surfaces. *IEEE Trans. on Ant. and Prop.* **February 1994**, *42* (2), 220–231.

7. Beckman, P. Scattering by Non-Gaussian Surfaces. *IEEE Trans. on Ant. and Prop.* **March 1973**, *21* (2), 169–175.

8. Kodis, R. D. A Note on the Theory of Scattering from an Irregular Surface. *IEEE Trans. on Ant. and Prop.* **January 1966**, *14* (1), 77–82.

9. Barrick, D. E. Rough Surface Scattering Based on the Specular Point Theory. *IEEE Trans. on Ant. and Prop.* **July 1968**, *16* (4), 449–454.

10. Brown, G. S. Backscattering from a Gaussian-Distributed Perfectly Conducting Rough Surface. *IEEE Trans. on Ant. and Prop.* **September 1969**, *17* (5), 472–481.

11. Swift, C. T. A Note on Scattering from a Slightly Rough Surface, *IEEE Trans. on Ant. and Prop.* **July 1971**, *19* (4), 561–562.

12. Ulaby, F. T.; Elachi, C.; ed. *Radar Polarimetry for Geoscience Applications*; Artech House: Norwood, Mass., 1990.

13. Bahar, E.; Lee, B. S. Full Wave Solutions for Rough Surface Bistatic Radar Cross Sections – Comparison with Small Perturbation, Physical Optics, Numerical and Experimental Results, Radio Science **1994**, *29* (2), 407 – 429.

14. Pizzillo, Thomas, J.; Wellman, Ronald. *High-Range Resolution Profiles and RCS Measurements of Three Canonical Shapes at K_a-Band*; ARL-TR-2947; Army Research Laboratory: Adelphi, MD, May 2003.

15. Pizzillo, Thomas, J. *High-Range Resolution Profiles and Radar Cross Section (RCS) Measurements of Five Kinetic Energy Penetrators at K_a-Band (U)*; ARL-TR-3172; Army Research Laboratory: Adelphi, MD, May 2004, SECRET.

16. Bossoli, R. B. The Microwave Permittivity of Mil.-Spec. Primers and CARC Paints. Army Research Laboratory, March 2004 (in press).

17. Bhattacharyya, A. S.; Tandon, S. K. Radar Cross Section of a Finite Planar Structure Coated with a Lossy Dielectric. *IEEE Trans. on Ant. and Prop.* **September 1984**, *32* (9), 1003–1007.

18. Coburn, W. O.; Le, C. D.; Kenyon, C. S.; Spurgeon, W. A.; Carter, S. L. *The RCS of a Canonical Corner Target Including Lossy Dielectric Materials*; ARL-TR-3112; Army Research Laboratory: Adelphi, MD, November 2003.

Distribution List

ADMNSTR
DEFNS TECHL INFO CTR
ATTN DTIC-OCP (ELECTRONIC COPY)
8725 JOHN J KINGMAN RD STE 0944
FT BELVOIR VA 22060-6218

DARPA
ATTN IXO S WELBY
3701 N FAIRFAX DR
ARLINGTON VA 22203-1714

INST FOR DEFNS ANLYS SCI &
TECHLGY DIV
ATTN J T FRASIER
1801 N BEAUREGARD STRET
ALEXANDRIA VA 22311-1772

OFC OF THE SECY OF DEFNS
ATTN ODDRE (R&AT)
THE PENTAGON
WASHINGTON DC 20301-3080

US ARMY TRADOC
BATTLE LAB INTEGRATION & TECHL
DIRCTRT
ATTN ATCD-B
10 WHISTLER LANE
FT MONROE VA 23651-5850

CMDR
HDQTRS DEPT OF THE ARMY
ATTN DAMI-FIT
NOLAN BLDG
WASHINGTON DC 20301-0430

PM COMBAT SYS
ATTN SFAE-ASM-AB
6501 ELEVEN MILE RD
WARREN MI 48397-5000

SMC/GPA
2420 VELA WAY STE 1866
EL SEGUNDO CA 90245-4659

US ARMY ARDEC
ATTN AMSTA-AR-TD
BLDG 1
PICATINNY ARSENAL NJ 07806-5000

US ARMY ARDEC INTLLGNC
SPECIALIST
ATTN AMSTA-AR-WELL-F M
GUERRIERE
PICATINNY ARSENAL NJ 07806-5000

COMMANDING GENERAL
US ARMY AVN & MIS CMND
ATTN AMSAM-RD W C MCCORKLE
REDSTONE ARSENAL AL 35898-5000

US ARMY AVN & MIS CMND
COMANCHE PROGRAM MGMT OFC
ATTN SFAE-RAM-TV D CALDWELL
BLDG 5681
REDSTONE ARSENAL AL 35898

US ARMY INFO SYS ENGRG CMND
ATTN AMSEL-IE-TD F JENIA
FT HUACHUCA AZ 85613-5300

US ARMY MATERIEL CMND
ATTN AMXMI-INT
9301 CHAPEK RD
FT BELVOIR VA 22060-5527

US ARMY NATICK RDEC
ACTING TECHL DIR
ATTN SBCN-TP P BRANDLER
KANSAS STREET BLDG 78
NATICK MA 01760-5056

US ARMY NATL GROUND INTLLGNC CTR
ATTN J SIZEMORE
2055 BOULDERS RD
CHARLOTTESVILLE VA 22911-8318

US ARMY PM M2/M3 BFVS
ATTN SFAE-GCSS-W-BV
WARREN MI 48397-5000

US ARMY RDECOM TARDEC
ATTN AMSRD-TAR-R D THOMAS
MS 263
6501 E. ELEVEN MILE RD
WARREN MI 48397-5000

US ARMY SIMULATION TRAIN & INSTRMNTN CMND
ATTN AMSTI-CG M MACEDONIA
12350 RESEARCH PARKWAY
ORLANDO FL 32826-3726

US ARMY TACOM
ATTN AMSTA-TR-D D OSTBERG
ATTN AMSTA-TR-R T GONDA
WARREN MI 48397-5000

US ARMY TARDEC
ATTN AMSTA-TR-R J BENNETT
MS263
WARREN MI 48397-5000

NAV SURFC WARFARE CTR
ATTN CODE B60 TECHL LIB
17320 DAHLGREN RD
DAHLGREN VA 22448-5100

GENERAL DYNAMICS AMPHIBIOUS SYS
ATTN SURVIVABILITY LEAD G WALKER
991 ANNAPOLIS WAY
WOODBRIDGE VA 22191

GENERAL DYNAMICS LAND SYS
ATTN M PASIK
PO BOX 1800
STERLING HEIGHTS MI 48090-1800

GENERAL DYNAMICS LAND SYS
MUSKEGON OPERATIONS
ATTN M SOIMAR
76 GETTY ST
MUSKEGON MI 49442

HICKS & ASSOC INC
ATTN G SINGLEY III
1710 GOODRICH DR STE 1300
MCLEAN VA 22102

PALISADES INST FOR RSRCH SVC INC
ATTN E CARR
1745 JEFFERSON DAVIS HWY STE 500
ARLINGTON VA 22202-3402

SAIC HUNTSVILLE
ATTN D RAINS
ATTN J COOK
6725 ODYSSEY DR NM
HUNTSVILLE AL 35806

SAIC-DEMACO
ATTN K WELSH
ATTN S KASANOVICH
1901 S FIRST ST STE D1
CHAMPAIGN IL 61820

UNITED DEFNS LIMITED PARTNERS
ATTN R BRYNSVOLD
4800 EAST RIVER RD
MINNEAPOLIS MN 55421-1498

US ARMY RSRCH LAB
ATTN AMSRD-ARL-CI-HC E MARK
ATTN AMSRD-ARL-SE-RM R BENDER
ATTN AMSRD-ARL-SE-RM S STRATTON

US ARMY RSRCH LAB (cont'd)
ATTN AMSRD-ARL-WM-BC P PLOSTINS
ATTN AMSRD-ARL-WM-MA S MCKNIGHT
ATTN AMSRD-ARL-WM-MB C HOPPEL
ATTN AMSRD-ARL-WM-MB L BURTON
ATTN AMSRD-ARL-WM-MB R BOSSOLI
ATTN AMSRD-ARL-WM-MB R LIEB
ATTN AMSRD-ARL-WM-MB S CORNELISON
ATTN AMSRD-ARL-WM-MB W DRYSDALE
ATTN AMSRD-ARL-WM-MB W SPURGEON
ATTN AMSRD-ARL-WM-MD W ROY
ATTN AMSRD-ARL-WM-T B BURNS
ATTN AMSRD-ARL-WM-TC R COATES
ABERDEEN PROVING GROUND MD 21005

US ARMY RSRCH LAB
ATTN AMSRD-ARL-CI-HC R NAMBURU
ABERDEEN PROVING GROUND MD 21005-5006

US ARMY RSRCH LAB
ATTN AMRSD-ARL-WM-MB M MAHER
ATTN AMSRD-ARL-SE-RM R TAN
ATTN AMSRD-ARL-WM-BA D LYONS
ATTN AMSRD-ARL-WM-TE A NIILER
ABERDEEN PROVING GROUND MD 21005-5066

DIRECTOR
US ARMY RSRCH LAB
ATTN AMSRD-ARL-RO-D JCI CHANG
PO BOX 12211
RESEARCH TRIANGLE PARK NC 27709

US ARMY RSRCH LAB NASA LANGLEY RSRCH CTR VEHICLE TECHLGY CTR
ATTN AMSRD-ARL-VT W ELBER
HAMPTON VA 23681-0001

US ARMY RSRCH OFC
ATTN J PRATER
PO BOX 12211
RESEARCH TRIANGLE PARK NC 27709-2211

US ARMY RSRCH LAB
ATTN AMSRD-ARL-CI-OK-T TECHL PUB (2 COPIES)
ATTN AMSRD-ARL-CI-OK-TL TECHL LIB (2 COPIES)
ATTN AMSRD-ARL-D J M MILLER
ATTN AMSRD-ARL-SE-RM E BURKE
ATTN AMSRD-ARL-SE-RU A SULLIVAN
ATTN AMSRD-ARL-SE-RU C KENYON
ATTN AMSRD-ARL-SE-RU C LE
ATTN AMSRD-ARL-SE-RU T DOGARU
ATTN AMSRD-ARL-SE-RU W O COBURN
ATTN AMSRL-SE-RU B STANTON (5 COPIES)
ATTN AMSRL-SE-RU M QAADRI
ATTN IMNE-ALC-IMS MAIL & RECORDS MGMT
ADELPHI MD 20783-1197

INTENTIONALLY LEFT BLANK.